

Narasimhan Desigan, Nirav Bhatt, Madhuri A. Shetty, Gopala Krishna Pillai Sreekumar, Niranjan Kumar Pandey, Uthandi Kamachi Mudali, Rajamani Natarajan and Jyeshtharaj B. Joshi*

Dissolution of nuclear materials in aqueous acid solutions

<https://doi.org/10.1515/revce-2017-0063>

Received July 24, 2017; accepted May 24, 2018

Abstract: The quantitative understanding of the dissolution of nuclear fuel materials is essential for the process design and development of an industrial-scale nuclear fuel reprocessing plant. The main objective of this review article is to analyze the published data related to the dissolution of important nuclear materials, namely, urania, plutonia, thoria, and their oxides in the existing literature. The published results on rate-controlling step and reaction mechanism of dissolution processes are reconciled and reviewed in this work. Clear suggestions are made for future research work for the identification of rate-controlling step. Suggestions are also provided to overcome the shortfalls in the published data for the identification of intrinsic kinetics and mass-transfer rates.

Keywords: aqueous processing; nuclear fuel reprocessing; reaction kinetics; reactive dissolution.

1 Introduction

1.1 Preamble

In developing countries, the demand for power is ever increasing. In the current state of scenario, most of the energy resources are slowly approaching exhaustion. Nuclear energy, with its breeding capability using fast breeder reactor (FBR) technology, is a very attractive option

to partially meet this requirement. Hence, this technology has been gaining more importance in the last three decades with the advent of all of its new developments. Among all the operations in a closed fuel cycle, reprocessing of fuel is the most important step as it is where the unirradiated and the newly bred fissile materials are recovered from spent fuel. Only when the spent fuel is reprocessed that the breeding capability of a fast reactor is realized. The success of a reprocessing plant depends on the level of recovery of the fissile material with minimum generation of radioactive wastes. Thus, the handling of spent fuel is an important unit operation in the nuclear fuel cycle. The reprocessing of spent fuel is one of the options towards long-term management of spent fuel with the simultaneous demonstration of peaceful use of atomic energy. This is because reprocessing recovers valuable materials that can be reused rather than wasted. Also, it facilitates the compacting of nuclear waste through subsequent fuel cycle operations. Two types of reprocessing technologies are used in practice: (i) aqueous processing and (ii) pyrochemical processing (Bodansky 2006). As of date, commercial reprocessing operations have been achieved only through aqueous routes in industries worldwide. The technology is well established, proven, and matured for handling spent oxide fuels. It has been also demonstrated successfully for processing other advanced nuclear fuels like plutonium-rich mixed carbide fuel (Natarajan et al. 2015). On the other hand, pyrochemical methods have been used only in the pilot scale for research and development (R&D) purposes. The technology is yet to mature for commercial scale operations (Poinssot et al. 2012b).

1.2 Aqueous processing

In commercial aqueous reprocessing, chopped spent fuel is dissolved in nitric acid, and the dissolved uranium (U) and plutonium (Pu) in the aqueous phase are recovered by liquid-liquid extraction process. PUREX (plutonium and uranium extraction) process is one of the most widely employed methods for reprocessing the spent fuel. In the PUREX process, U and Pu are dissolved in nitric acid as U(VI) and Pu(IV) nitrates and are extracted using tributyl phosphate (TBP) (Sood and Patil 1996, Olander 2009).

*Corresponding author: Jyeshtharaj B. Joshi, Homi Bhabha National Institute, Anushaktinagar, Mumbai, 400094, India; and Department of Chemical Engineering, Institute of Chemical Technology, Mumbai, 400019, India, e-mail: jbjoshi@gmail.com

Narasimhan Desigan, Niranjan Kumar Pandey, Uthandi Kamachi Mudali and Rajamani Natarajan: Department of Atomic Energy, Reprocessing Group, Indira Gandhi Centre for Atomic Research, Kalpakkam, 603102, India

Nirav Bhatt: Department of Chemical Engineering, Indian Institute of Technology Madras, Chennai, 600 036, India

Madhuri A. Shetty and Gopala Krishna Pillai Sreekumar: Department of Atomic Energy, Bhabha Atomic Research Centre, Trombay, Mumbai, 400094, India

This step is followed by scrubbing, precipitation, and calcination to obtain highly purified U and Pu oxides. The purified Pu and U oxides are then mixed in definite proportions and recycled as mixed oxide (MOX) fuel. To prevent the proliferation of Pu, UREX (uranium recovery by extraction), a variant of PUREX, is developed to extract only U from spent fuel (Thompson et al. 2002). There is a push to develop advanced aqueous processing such that it is proliferation-resistant. There are other solvent extraction processes such as SREX, TRUOX, DIAMOX, UNEX, COEX, GANEX, etc., which are being used to extract other actinides (Romanovskiy et al. 2001, Hill et al. 2002, Rat and Heres 2004, Ackerman 1991, Aneheim 2012, COE 2017) such as Am, Np, and Cm from the high-level liquid wastes generated in PUREX process for facilitating long-term liquid waste management in the nuclear industries.

1.3 Pyrochemical processing

In pyrochemical processing, molten mixture of LiCl-KCl is used to melt the spent fuel. Then, U, Pu, and other actinides are separated using the electrorefining process (Ackerman 1991, Laidler et al. 1997, Bodansky 2006). This method is often called “dry reprocessing” and has been originally conceptualized by Argonne National Laboratory (Bodansky 2006). The process is intrinsically proliferation-resistant due to the difficulty in extracting weapon-grade Pu using this approach. Furthermore, the pyrochemical processes are capable of handling highly irradiated fuel in comparison to the aqueous processes. These methods can make reprocessing facilities compact and the ability to work with the spent fuel with shorter cooling period as compared to the aqueous processing (OECD 2004). Although pyrochemical processing is a promising alternative to aqueous processing, it is still to be commercialized on a wider scale as the process has not yet matured enough on a large scale.

1.4 Motivation of current review

Aqueous processing is the state of the art in commercial spent fuel reprocessing. A better understanding of various aspects of this process is desirable for better plant performance and economics. Reactive dissolution is one of the most important operations in the management of spent fuel via aqueous processing. Hence, the qualitative and quantitative understanding of this operation is essential for process design and development at an industrial scale. There are several studies to understand the

mechanism of the dissolution of nuclear materials such as uranium oxide and plutonium oxide in the existing literature (Taylor et al. 1963, Shabbir and Robins 1968, Barney 1977). These studies attempted to develop qualitative as well as quantitative understanding of these dissolution processes. These studies included information regarding various parameters such as roles of surface area, additives, extents of mixing, effect of pressure, temperature, concentration of reactive solvent, etc. Moreover, some of these studies have also developed kinetic models. However, these studies need to be revisited because the individual role of mass transfer and chemical reactions need to come out clearly. For the rational procedure for scale-up, it is desirable to have the knowledge of intrinsic kinetics. For this purpose, the dissolution processes can be adequately described via model-based analysis of experimental data (Marquardt 2005). Hence, before designing costly, new set of experiments to develop an adequate understanding of these processes, it is always advisable to analyze and to reconcile the existing results in the literature.

In this work, the dissolution of urania (UO_2), plutonia (PuO_2), thoria (ThO_2), and their MOXs in acids will be presented using analysis of the published data in the existing literature. The effect of additives such as KF, Ce(IV), NaNO_2 , HF, etc. on the dissolution will also be included in the quantitative modelling. The published data will be used to reconcile and identify information regarding reaction kinetics and mass transfer rates. Care will be taken to include possible changes in the structure of solids, particle size distribution, and morphology. The expression of reaction kinetics and activation energy will be estimated based on the experimental data. The estimated values will be compared to draw some general conclusions on achievements and shortfalls of the published work. Furthermore, clear suggestions will be made for future research work for the identification of rate-controlling step and the determination of design of new experiments to overcome the shortfalls of the published data.

The article is organized as follows. First, mathematical modelling approach of reactive dissolution is given. Then, the results of the analysis of experimental data in the existing literature are discussed for three types of oxides. Based on the results obtained from the analysis of the published data, several suggestions are made for developing quantitative models based on optimal design of experiments and industrial dissolvers. As emphasis is given for the industrial reprocessing methods in this work, only the conventional processes for the dissolution of nuclear fuel are considered here. Other methods such as electrochemical, ultrasound based, and photo-chemical are only briefly mentioned for the sake of completion, as

these technologies are still at research stages and will take time to reach commercial stage.

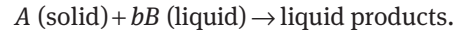
2 Mathematical modelling of reactive dissolution: chemical reactions with mass transfer

In reactive dissolution of oxides, the reactants in the liquid phase transfer to the solid surface, and the chemical reactions take place on the surface of the solid particles (for porous materials, inside the pores). For simplicity of the presentation, it is assumed that the reactions take place only on the surface. Then, the dissolution of the desired material(s) is accomplished by the following steps: (i) the mass transfer of the reactants through the liquid film, (ii) the chemical reactions on the surface of the solid, (iii) the desorption of the products from the surface, and (iv) the mass transfer of products through the liquid film (Wen 1968, Levenspiel 1999). The shrinking particle model is an appropriate method for describing reactive dissolution of oxides. In this model, it is assumed that the particle size steadily decreases as the reactions proceed (typically expressed as a function of conversion). This approach assumes the ideal geometries of solid and the reaction kinetics (first or second order) to develop models that typically describe the change in the ratio of the initial radius to the radius and the conversion of the solid phase at any time t (Dickinson and Heal 1999, Grénman et al. 2011a,b). Interested readers can find a list of such models (ideal geometry, reaction kinetics) in the literature (Dickinson and Heal 1999, Órfão and Martins 2002, Grénman et al. 2011a,b). In practice, the shapes of solid particle are far from the ideal geometries. Furthermore, reaction rates can be modelled other than the power-law kinetics, for example, inhibition kinetics, autocatalytic, etc. Hence, fitting the data from dissolution experiments to these oversimplified models may lead to unreliable models and misinterpretation of the values of parameters (Grénman et al. 2011a). It is important to address these issues in modelling of reactive dissolution systems for developing a reliable model from experimental data.

2.1 Modelling of batch reaction systems with mass transfer

Next, we describe mathematical modelling of batch solid-liquid reaction systems involving the dissolution of single

component of solid in the aqueous liquid. The following reaction takes place on the solid surface:



Consider particles of component A having surface area A_s reacting with component B in a continuously stirred liquid. It is assumed that the solid and liquid phases are in batch mode of operations. In order that component B reacts with component A , it follows steps (i), (ii), and (iii) described in the previous section. Then, the liquid products desorb from the surface via step (iv). Furthermore, it is assumed that there is no accumulation in the liquid film surrounding the solid particles. The mole balances for component B in the liquid bulk ($n_{l,B}$) and in the solid particle ($n_{s,B}$) and component A ($n_{s,A}$) can be written as follows:

$$\begin{aligned} \frac{dn_{l,B}}{dt} &= -N_B A_s \\ \frac{dn_{s,B}}{dt} &= N_B A_s - b r_1 A_s \\ \frac{dn_{s,A}}{dt} &= -r_1 A_s \end{aligned} \quad (1)$$

where N_B is the mass transfer rate of component B from the bulk to the solid surface ($\text{mol s}^{-1} \text{m}^{-2}$), r_1 is the rate of reaction ($\text{mol s}^{-1} \text{m}^{-2}$), A_s the surface area (m^2), and b the stoichiometric. Note that a reaction rate is a function of concentrations of reactants. The mole balance for the j th product ($j=1, \dots, P$) on the solid surface ($n_{s,j}$) and the liquid bulk ($n_{l,j}$) can be expressed as follows:

$$\begin{aligned} \frac{dn_{s,j}}{dt} &= -N_j A_s + p_j r_1 A_s \\ \frac{dn_{l,j}}{dt} &= N_j A_s \end{aligned} \quad (2)$$

where N_j is the mass transfer rate of the j th product from the solid surface to the bulk liquid and p_j is the stoichiometric coefficient of the j th product. For developing a reliable model, the intrinsic kinetics (r_1), mass transfer rates (N_j , $j=B, 1, \dots, P$), and the effect of particle surface area (or morphology) (A_s) in Eqs. (1) and (2) need to be identified based on experimental data. For the shrinking particle size without the product layer formation, the reaction kinetics and the mass transfer from the liquid bulk to the solid surface are two rate-controlling steps. If mass transfer to the surface is very fast compared to the reaction kinetics, then the overall rate of the underlying system is controlled by the intrinsic kinetics and vice versa. Two cases of rate-controlling steps are described below.

2.1.1 Chemical reaction control

For this case, there is no accumulation of component B on the surface, i.e. $\frac{dn_{l,B}}{dt} = 0$. Thus, Eq. (1) can be written as follows:

$$\frac{dn_{s,B}}{dt} = -b \frac{dn_{s,A}}{dt} = -br_1 A_s \quad (3)$$

For the first-order kinetics in terms of bulk concentration ($c_{l,B}$) and single spherical particle, the conversion-time model is given as follows Levenspiel (1999):

$$\frac{t}{\tau} = 1 - (1 - X)^{1/3} \quad (4)$$

where t is time, $\tau = \frac{R\rho_A}{bk_r c_{l,B}}$ is the time required for the complete conversion, ρ_A is the density of solid, R is the initial diameter of solid sphere, k_r is the kinetic rate constant, and X is the fractional conversion at any time t (Levenspiel 1999). Note that the model in Eq. (4) can be applied to the systems having first-order kinetics. Hence, its application to the systems following kinetics other than the first order leads to inaccurate interpretation of the data. In practice, reaction kinetics can be identified as follows: (i) postulate candidate kinetic expressions for each reaction, for example, power-law, inhibition kinetics, etc.; (ii) include all other steps for getting overall rate of reaction; (iii) fit each candidate expression (overall rate equations) to the experimental (or computed) rate data; and (iv) choose the best fitting candidate expression as a reliable reaction kinetic expression. Interested readers can find the details of such methodological approaches in the studies by Marquardt (2005) and Grénman et al. (2011b).

2.1.2 Mass-transfer control

In this case, the reaction proceeds fast in comparison to the mass transfer of component B from the liquid bulk to the surface. Then, the mass transfer is the rate-controlling step and the mass-transfer rate depends on the driving force ($c_{l,B} - c_{s,B}$), size of the particle, relative velocity between particle and the liquid phase, and the liquid properties. Note that the concentration of B is approximately zero on the solid surface. Thus, Eqs. (1)–(3) can be written as follows:

$$\frac{dn_{l,B}}{dt} = b \frac{dn_{s,A}}{dt} = -k_l c_{l,B} A_s \quad (5)$$

where k_l is a mass-transfer coefficient, which is a function of various hydrodynamics variables and the properties of the liquid. It is expressed in terms of relationship among Sherwood number (N_{Sh}), Reynold number (N_{Re}), and Schmidt number (N_{Sc}). For example, Frossling correlation is one of the most widely used relationships in the literature and is given as (Levenspiel 1999):

$$N_{Sh} = 2 + 0.6 N_{Re}^{1/2} N_{Sc}^{1/3} \quad (6)$$

$$\frac{k_l d_p}{D} = 2 + 0.6 \left(\frac{d_p u \rho_l}{\mu} \right)^{1/2} \left(\frac{\mu}{D \rho_l} \right)^{1/3}$$

where d_p is the diameter of the particle, u is the relative velocity of the liquid, ρ_l is the density of the liquid, μ is the viscosity, and D is the diffusivity. Hence, k_l varies as the reaction proceeds because of the change in the particle size.

In practice, the dissolution rate is a combination of the mass-transfer and the kinetic resistances. The contribution of the different resistances may vary as the reaction proceeds. Furthermore, the effect of the solid shape and surface area, and temperature also plays an important role in reactive dissolution. Their effects are discussed in the following sections.

2.1.3 Solid shape and surface area

The surface area in solid-liquid reactions explains the order of reaction with respect to the solid phase (Grénman et al. 2011b). The standard models do not take into account the irregular shapes, and hence, they cannot be applied to the irregularly shaped solids. To include the irregular geometries and porous material, it is proposed to use shape factors (Grénman et al. 2011b, Salmi et al. 2011) so that surface area can be expressed in terms of the solid numbers of moles and the shape factor as follows (Salmi et al. 2011):

$$A_s = \frac{aM}{\rho_s R_0} n_{s,0}^x n_s^{1-x} \quad (7)$$

where a is the shape factor; M , molecular weight; ρ_s , the solid density; R_0 , the initial characteristic dimension of the solid particle; and $x = 1/a$. Table 1 describes the particle geometry and the corresponding shape factor and x values (Grénman et al. 2011b). Note that irregularities such as rough surface, porosity, etc. increase the order of the reaction with respect to solid particles.

Table 1: Particle geometry, shape factor, and x for different geometries (Grénman et al. 2011b).

Geometry	Shape factor (a)	x	$1-x$
Slab	1	1	0
Cylinder	2	1/2	1/2
Sphere	3	1/3	2/3
Irregular particle	$a \rightarrow \text{inf}$	$1/a \rightarrow 0$	$\rightarrow 1$

2.1.4 Temperature

Temperature plays an important role for the systems that are kinetically controlled. The effect of temperature can be modelled by the Arrhenius equation as follows:

$$k_r = k_0 \exp\left[-\frac{E_i}{R_g T}\right] \quad (8)$$

where k_r is the pre-exponential factor; E_i , the activation energy for the i th reaction; R_g , the universal gas constant; and T , the temperature in Kelvin.

2.1.5 Particle size distribution (PSD)

In this section, it is assumed that all the particles are of the same size. However, in practice, the particles are often of different sizes, and hence, the overall rate of reaction in the dissolver is different from the rate computed under the assumption of the mean particle size. Hence, PSD should be used to compute the overall rate instead of the mean size of particle.

3 Dissolution of three oxides

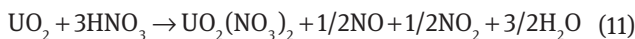
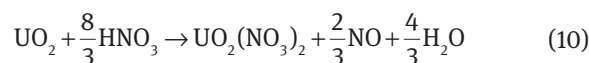
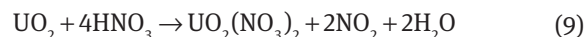
In this section, the objective is to reconcile the existing results and analyze the published data to bring out the gaps if they exist. The published data on three dioxides (UO_2 , PuO_2 , and ThO_2) are analyzed in this section. The kinetic models are fitted to estimate the order of reactions and activation energies. As the insoluble residues do not affect the dissolution significantly, the analysis of the insoluble residues is not taken into consideration for evaluating the dissolution process. These residues have more implications on the solvent extraction processes, which are the next unit operation in the reprocessing of spent fuel for the recovery of fissile nuclides.

3.1 Dissolution of uranium dioxide

In this section, various aspects of the dissolution of uranium dioxide will be reviewed. These aspects are listed as follows: (i) reaction kinetics and mechanism, (ii) effect of stirring speed, (iii) effect of additives, and (iv) role of surface area and pellet shapes. For each of these aspects, the available published information has been analyzed and presented here.

3.1.1 Reaction kinetics and mechanism

Uranium dioxide dissolves rapidly in HNO_3 in comparison to plutonium or thorium dioxides. Several attempts in existing literature were made to understand the reaction mechanism of dissolution and the kinetics in terms of orders of reaction and activation energy (Shabbir and Robins 1968, 1969, Ikeda et al. 1995). It has been proposed that UO_2 dissolves in HNO_3 via one of the following reactions (Uriate and Rainey 1965):



The experimental data from several publications, including our recent work (Desigan et al. 2015a, 2017) have been analyzed to compute activation energies and order of reaction with respect to HNO_3 . These results, along with the published values, are given in Table 2. Note that these data are collected in the kinetic controlled zone by carefully eliminating the effect of stirring speed during the experiments.

The computed and published activation energies are in the range of 50–80 kJ mol^{-1} , suggesting that the dissolution of uranium dioxide is kinetically controlled (Yu and Ji 1992). Moreover, the order of reaction with respect to HNO_3 (or NO_3^{-}) is in the range of 2.3–3.2 for most of the cases, which was also suggested by Taylor et al. (1963). However, the activation energies and orders of reaction computed by Shabbir and Robins (1968, 1969) deviate substantially from the abovementioned range of 50–80 kJ mol^{-1} for powder and pellet. For Shabbir and Robins (1969), the activation energy value of 30.6 kJ mol^{-1} and the order of 1.21 indicate the significant presence of mass transfer resistance in the experimental data. These values can also be due to lower concentration range of

Table 2: Summary of results obtained via analysis of experimental data in the published literature for UO_2 .

Authors	Shape and size of UO_2	Activation energy (kcal mol ⁻¹)	Order of reaction	Conc. HNO_3 (M)
Taylor et al. (1963)	Pellet (-)	11.47	2.27	3–10
Stirred run		[12]	–	
Published		13.44	2.43	
Unstirred run		[14.8 ± 1.3]	[2.8 ± 0.5]	
Published				
Uriate and Rainey (1965)	Pellet (D = 1.06 cm, L = 1.59 cm)	–	2.3	2–10
Shabbir and Robins (1968)	Powder	7.33	1.21	0.5–2
	(0.003–0.3 μm)	16.68	1.76	2–10
	Sphere			
	(100–500 μm)			
Shabbir and Robins (1969)	Pellet (D = 0.25 in, L = 0.75 in)	25.6 (650 psi)	3.3	4–10
Inoue and Tsujino (1984)	U_3O_8 Powder	16.94	1.9	4–10
Published	(4.8 μm)	[14–19]		
Fukasawa and Ozawa (1986)	Pellet (D = 1 cm, L = 1.1 cm)	–	3.2	7.3 (initial)
Published			[2.8]	
Ikeda et al. (1995)	Powder (300–350 μm)	14.22	2.74–2.94	6–9.5
Published		[18.9 ± 1.6]	2.3	
Pierce (2004)	Scrap (U)	16.5	3.4	2–10
Published			3	
Mineo et al. (2004)	Pellet	14.27	2.13	5 (initial)
Published	(L = 0.04 m)	[14.5]	[2]	
Cordara et al. (2017)	Pellet	5.82	4.44	0.1–4
	(D = 0.5 cm)			

The computed activation energies and order of reaction are compared with those published in the article (denoted as Published in the table).

HNO_3 , which was employed in these experiments. Furthermore, the authors used UO_2 powder in these experiments. In the case of pellet, the authors had performed experiments at higher pressure. The results in Table 2 also indicate that the order of reaction increases with an increase in particle size. Moreover, at low HNO_3 concentration (0.5–2 M), the behavior of UO_2 dissolution is different from that at relatively higher concentrations (2–10 M).

It was observed that the activation energy computed for the stirred runs of Taylor et al. (1963) is lower than the one computed for the unstirred runs. These values are in line with those reported by Taylor et al. (1963). They attributed the reduction in dissolution rate to an autocatalytic nature of process and the possible role of nitrous acid as an autocatalytic product. The same observation was also made by Shabbir and Robins (1968, 1969), Inoue and Tsujino (1984), and Desigan et al. (2015a). They mentioned that the role of reduction products such as NO , NO_2 , and HNO_2 should be considered for understanding the underlying reaction mechanism. Ikeda et al. (1995) studied the role of HNO_2 in the dissolution of UO_2 and concluded that the dissolution of UO_2 in HNO_3 depends on the concentration of HNO_2 on the surface of solid. They proposed that the dissolution proceeds through

two paths and the rate of reaction (r) can be written as follows:

$$r = (k_1 + k_2 C_{\text{HNO}_2}) C_{\text{HNO}_3}^{2.3} \quad (12)$$

In Eq. (12), path k_1 is independent of C_{HNO_2} , while path k_2 depends on C_{HNO_2} . Equation (12) can be used to explain the role of HNO_2 in the dissolution process and the difference in activation energies for the unstirred and stirred runs over a wide range of high concentrations and temperatures. For the unstirred runs, C_{HNO_2} is higher at the surface of UO_2 . The increase in the stirring speed facilitates the diffusion of HNO_2 from the surface to the liquid bulk, and consequently, C_{HNO_2} on the surface decreases at the higher speed. Hence, the contribution of path k_2 decreases, leading to a lower overall rate of reaction and lower activation energy for the stirred runs. Moreover, they explained the lower activation energy at high temperature and HNO_3 concentration via the decomposition reaction of HNO_2 . At these conditions, the decomposition reaction, $2\text{HNO}_2(\text{l}) \rightarrow \text{NO}(\text{g}) + \text{NO}_2(\text{g}) + \text{H}_2\text{O}(\text{l})$ is fast and leads to lower concentration of HNO_2 . Hence, it decreases the overall dissolution rate. However, Eq. (12) is not completely in agreement with the observations of Taylor et al. (1963), as described below. At high temperatures and

concentrations, the contribution of path k_1 predominates, while that of path k_2 is negligible due to low concentration of HNO_2 . Hence, the activation energy should change to 79 kJ mol^{-1} (corresponding to path k_1). However, Taylor et al. (1963) noticed a significant drop in the activation energies ($8\text{--}21 \text{ kJ mol}^{-1}$). Hence, the exact role of HNO_2 on the overall rate needs to be revisited to confirm or refine Eq. (12).

3.1.2 Effect of stirring speed

The majority of kinetic studies in Table 2 were performed in kinetically controlled regimes, i.e. 100–500 rpm, speeds above which there is no noticeable effect of the stirring speed. As mentioned earlier, it is observed that the increase in the stirring speed decreases the dissolution rate as well as the activation energy (Taylor et al. 1963, Inoue and Tsujino 1984). This phenomenon indicates the autocatalytic reaction mechanism and the participation of one of the products as a catalyst. It is proposed that nitrous acid is acting as a catalyst in this process (Taylor et al. 1963, Inoue and Tsujino 1984, Ikeda et al. 1995). We have studied the dissolution kinetics of typical Indian PHWR sintered UO_2 pellets in nitric acid (Desigan et al. 2015b). Our results on dissolution kinetics also confirm this observation.

3.1.3 Effect of additives

Uranium dioxide dissolves rapidly in HNO_3 without additives compared to plutonium or thorium dioxide. However, several additives such as hydrogen fluoride (HF), aluminum nitrate ($\text{Al}(\text{NO}_3)_3$), sodium nitrate (NaNO_3), lithium nitrate (LiNO_3), uranyl nitrate ($\text{UO}_2(\text{NO}_3)_2$), and sodium nitrite (NaNO_2) were added to study their effects on the dissolution rate.

It was observed that the addition of HF increases the instantaneous dissolution rate (IDR) for HNO_3 concentration below 6 M. However, the IDR decreases with an increase in the HF concentrations above 6 M HNO_3 (Uriate and Rainey 1965). Often, $\text{Al}(\text{NO}_3)_3$ is added to HNO_3 -HF solutions to prevent corrosion. However, it is observed that aluminum nitrate nullifies the effect of HF on the dissolution rate. In our analysis, we fitted power-law kinetics to the IDR versus concentration data reported by Uriate and Rainey (1965), and it is found that the rate is proportional to the 3.06th power of HF concentration, the -2.97 th power of $\text{Al}(\text{NO}_3)_3$ concentration, and the 1.81th power of HNO_3 concentration. This analysis confirms the observation

made by Uriate and Rainey (1965) that aluminum nitrate has negative effect on the IDR. The addition of sodium, lithium, and uranyl nitrate into HNO_3 solution increases the dissolution rate. The fitting of power-law kinetics to the rate versus concentration data suggests that the IDR is proportional to the 2.3th power of total nitrate concentrations in the solution. This result is in line with the observation made by several authors (Shabbir and Robins 1968, 1969). Moreover, Taylor et al. (1963) observed that the addition of NaNO_2 increases the dissolution rate while the addition of nitrite-neutralizers reduces the dissolution rate. These results indicate the catalytic effect of nitrous acid, as represented by Eq. (12). We have also found similar observations in our experiments wherein addition of hydrazine as masking agent for nitrous acid resulted in significant reduction in dissolution rates (Desigan et al. 2015b).

3.1.4 Role of surface area and particle shapes

Shabbir and Robins (1969) and Ikeda et al. (1995) noticed that small particles dissolve rapidly than the large ones do. This observation indicates that the dissolution rate depends on the surface area of UO_2 . It was also observed that the effective surface area changes as dissolution proceeds (Shabbir and Robins 1968). Moreover, the chopped spent fuels in practice consist of cracks, shallow pitting, and minute pores (Fukasawa and Ozawa 1986, Mineo et al. 2004). The scanning electron microscopy of a 50% dissolved pellet indicates a rough surface area with open pores with diameter up to $100 \mu\text{m}$ (Fukasawa and Ozawa 1986). Furthermore, the effective surface area increases initially because more closed pores open up as dissolution proceeds. The effective surface area computed by submersion or mercury impregnation methods shows that effective surface area decreases monotonously after 20%–30% dissolution (Shabbir and Robins 1968, Fukasawa and Ozawa 1986). These observations indicate that the effective surface area needs to be incorporated to compute dissolution rate. Mineo et al. (2004) incorporated cracks in the spent fuels to compute the effective surface area.

Moreover, a comparison of dissolution rates among different shapes indicates that the dissolution rate in the case of powder is greater than that of spheres or pellets (Inoue and Tsujino 1984). They attributed this phenomenon to structural defects, such as high dislocation density, sharp edges, and corners in the case of powder. These results show the importance of morphology and lattice structure in dissolution processes.

3.1.5 Overall reaction mechanism

The role of nitrous acid as an autocatalytic reagent in the dissolution of sintered UO_2 pellets in nitric acid medium has been speculated on by many researchers (Taylor et al. 1963, Shabbir and Robins 1968, Inoue and Tsujino 1984), but none of the work mentioned in the literature gave any conclusive evidence for the reaction mechanism. Hence, Desigan et al. (2015a, 2017) carried out a detailed study to deduce the reaction mechanism of the same. Initially, the authors studied the effect of temperature and acidity on the reaction kinetics of sintered UO_2 pellet dissolution in nitric acid and estimated the activation energy (Desigan et al. 2015a, 2017). The reaction was found to be predominantly chemical reaction controlled. Subsequently, the authors studied the changes in pellet surface area and measured the composition of NO_x gases evolved during the course of dissolution as a function of time. The starting acidity in all the experiments was 8 M (Desigan et al. 2017). Eqs. (9)–(11) are the stoichiometric reactions taking place between UO_2 and nitric acid at various acid concentrations. These reactions predominantly take place in the acidity range above 8 M, between 6 and 8 M and below 6 M, respectively (Sakurai et al. 1988). The published results by Desigan et al. (2017) indicate that the ratio of C_{HNO_3} consumed to C_{U} dissolved is around 2.7 when the acidity of the reaction mixture is above 6 M, and the ratio changes to around 3 when acidity is below 6 M in all the experiments on the dissolution of sintered UO_2 pellets in the nitric acid medium. Based on the composition of NO_x gases measured during the course of dissolution, they observed that C_{NO} is always around 0.5–0.6 times that of C_{U} . Hence, in all experiments by Desigan et al. (2017), which were carried out under conditions prevailing in a typical PUREX process, the reaction depicted by Eq. (9) can be almost ruled out. It is only the reactions represented by Eqs. (10) and (11) that seem to be taking place most predominantly. C_{NO_2} was found to be very less until the acidity of the reaction mixture reaches 6 M. When the acidity of the reaction mixture crosses 6 M and dips further, there is sudden increase in C_{NO_2} . Furthermore, downtime until the completion of the dissolution process of C_{NO_2} continues to be hovering around C_{NO} , which is about half of C_{U} . This further emphasizes our conclusion that reaction (9) is negligible. The typical concentration profiles of nitrous acid and U in the bulk and NO_x gases evolved during the course of dissolution are given in Figure 1.

The overall reaction can be split into three zones time wise. In zone 1, as C_{NO} is about 0.6 times that of C_{U} , the reaction predominantly proceeds through either Eq. (10) or (11). As per Benedict et al. (1981), at higher acidities,

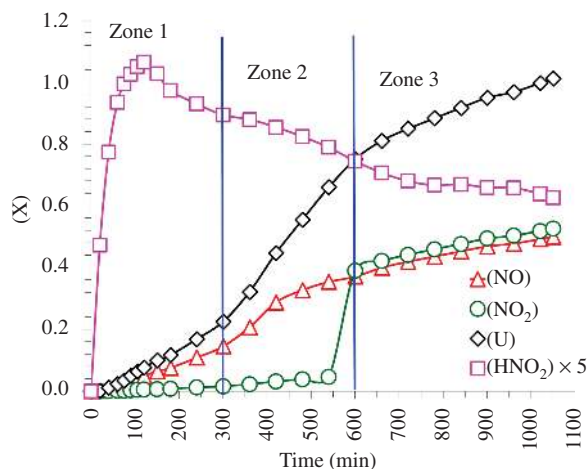
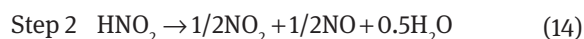


Figure 1: Typical concentration profiles of nitrous acid and U in the bulk and NO_x gases evolved during the course of dissolution.

the concentration of NO_2 in the NO_x stream will be higher. However, Desigan et al. (2017) found C_{NO_2} to be very less in the experiments. This is because NO_2 , due to its higher solubility in the aqueous phase (Joshi et al. 1985), reacts with water and forms HNO_2 . Hence, C_{HNO_2} increases in this zone. This confirms that the reaction taking place predominantly in time zone 1 (Figure 1) is Eq. (11). Nitrous acid formed decomposes quickly to NO_x gases.

Thus, the reaction takes place in two steps, as follows.



The NO_2 formed reacts quickly with water, as follows:

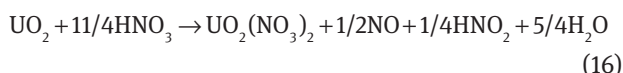


In time zone 2 (Figure 1), nitrous acid, which is produced at the pellet solution interphase, attains equilibrium, and it diffuses into the bulk of the reaction mixture at certain rate depending on the extent of agitation. The higher the agitation rate, the faster the diffusion of the nitrous acid, and, subsequently, it decomposes to NO and NO_2 , as represented in step 2 given in reaction (14). Also, in this time zone, as the pellet continues to become porous, which was inferred from the increasing total surface area of the sintered pellet, nitrous acid penetrates into these pores and accelerates the reaction further. Hence, C_{U} increases rapidly in this zone and, thereby, the dissolution rate.

In time zone 3, the pellet reduces in sufficiently smaller size due to the rapid dissolution in zone 2. As a result, the available surface for the reaction to take place is very less. Hence, the dissolution rate decreases, as indicated by the

decrease in the value of slope of C_u curve with time. At the same time, the reaction between NO_2 and water reaches equilibrium and attains steady state, leading to a constant slope in the C_{NO_2} plot with time.

Based on the above facts, the overall reaction mechanism can be summarized as follows. The sintered UO_2 pellet dissolves in nitric acid predominantly through reaction 11 in two steps, as indicated in Eqs. (13) and (14), under typical PUREX process conditions. NO_2 gas generated *in situ* reacts with water quickly leading to the formation of nitrous acid, as given in Eq. (15). The overall reaction is the algebraic addition of Eqs. 13–15, as follows:



Note that the above mentioned reaction mechanism operates irrespective of the reaction rate.

3.2 Dissolution of plutonium dioxide

3.2.1 Preamble

Fast reactor fuels typically contain Pu about 10–30% of the total heavy metal (THM), whereas for all the other types of reactors, it is relatively less. Thus, for the commercial success of the fast reactor fuel cycle technology, the dissolution of fast reactor spent fuel is a major step to be well explored. It is well known that uranium-based spent fuel dissolves rapidly in nitric acid under just heating in comparison to plutonium-based spent fuel, whereas addition of PuO_2 to UO_2 (making it MOXs) renders its dissolution sluggish in nitric acid (Goode 1965, Uriate and Rainey 1965, Schulz 1966, Horner et al. 1977). Hence, as Pu composition in the fuel increases, it becomes increasingly difficult to dissolve it in highly concentrated nitric acid just by heating. Once plutonium exceeds 35% of the THM, it was found to be difficult to dissolve it completely using nitric acid alone (Demuth 1997, Polley 2009). To enable the dissolution of such Pu-rich fuel, either electrolytic or addition of any strong complexing agents like hydrofluoric acid is normally required (Ryan and Bray 1980). When scrap materials with relatively high Pu are dissolved, which is normally a one-time campaign, the dissolver vessel is made of a special material like Ti or Zr to make it chemically strong enough to withstand the highly corrosive nature of the chemicals required to dissolve them.

Plutonium is known to exist in three different stable oxidation states, as follows: (III), (IV), and (VI), in the nitric acid medium depending on the acid concentration

(Fallet et al. 2016). Under typical PUREX process conditions, it co-exists in all these valency states. Pu(IV) is the most favorable oxidation state, which tributyl phosphate solvent extracts from nitric acid medium. Hence, after oxidative dissolution of PuO_2 , one has to reduce the resulting Pu(VI) ions to Pu(IV), which was found to be kinetically hindered in the nitric acid medium (Marchenko et al. 2009). On the other hand, the oxidation of Pu(III) to Pu(IV) is both a kinetically and thermodynamically favored process. This leads to the exploration of optimal methods for dissolution of PuO_2 . The experimental data from several publications have been analyzed to compute activation energies and order of reaction with respect to HNO_3 . These results along with the published values are given in Table 3.

3.2.2 PuO_2 dissolution in nitric acid

It has already been mentioned that, in contrast to UO_2 , PuO_2 dissolves in HNO_3 solution slowly. It was further observed that PuO_2 is practically insoluble in lower HNO_3 concentration (Uriate and Rainey 1965, Horner et al. 1977, Ryan and Bray 1980). Ryan and Bray (1980) showed this from a thermodynamic analysis. They justified the insolubility of PuO_2 in non-complexing nitric acid media based on the free energy calculations. They computed the standard free energy of PuO_2 dissolution reaction in nitric acid to be $\Delta G_{298}^0 = 41 \text{ kJ mol}^{-1}$ in low acidity (<5 M) and at the acid boiling point with the same concentration to be only slightly more favorable with $\Delta G_{373}^0 = -10.5 \text{ kJ mol}^{-1}$. Furthermore, it should be noted that the complexing constant of nitrate ions related to plutonium is low. They have to undertake (as a suggestion for future work) a systematic thermodynamic analysis to unravel the mechanism of PuO_2 dissolution. At relatively high concentrations (Uriate and Rainey 1965), it was observed that the IDR is proportional to the 4th power of HNO_3 concentration. For instance, in 10 M HNO_3 , the IDR of UO_2 pellet is $22.22 \text{ mg cm}^{-2} \text{ min}^{-1}$, while that of PuO_2 is $1 \times 10^{-3} \text{ mg cm}^{-2} \text{ min}^{-1}$.

3.2.3 PuO_2 dissolution in aqueous acids with fluoride promoters

The addition of small amount of fluoride promoters such as HF or KF in HNO_3 is the most widely used method to dissolve PuO_2 rapidly (Uriate and Rainey 1965, Harmon 1975a,b, Ryan and Bray 1980). Although the addition of HF increases initially the dissolution of PuO_2 by several fold, it slows down as the reaction progresses. One of the reasons might be the possible precipitation

Table 3: Summary of results obtained via analysis of experimental data in the published literature for PuO₂.

Authors	Shape	Activation energy (kJ mol ⁻¹)	Kinetic expression	Conc. HNO ₃ (M)	Additive	Surface area (m ² g ⁻¹)
Uriate and Rainey (1965)	Pellet	–	$kC_{\text{HNO}_3}^{4.05} C_{\text{HF},0}^{1.01}$	7–14	HF (0.0005–1)	7.3×10^{-5}
			$\frac{kC_{\text{HNO}_3}^{4.05} C_{\text{HF},0}^{0.37}}{C_{\text{Al(NO}_3)_3}^{0.025}}$	7–14	Al(NO ₃) ₃	
			$kC_{\text{HNO}_3}^{0.78} C_{\text{Ce(IV),0}}^{0.58}$	2–14	Ce(IV)	
			$kC_{\text{HNO}_3}^{-0.13} C_{\text{HCl},0}^{1.01}$		HCl	
Harmon (1975a,b)		NA		8	KF (0.05) Ce(IV) (0.0125–0.05)	Not known
Barney (1977)	Powder	13	kC_{HF}	10	HF (0.05–0.2)	2.9
Horner et al. (1977)	Microsphere	14.5	kC_{Ce}	1–13	Ce (0.03–0.12)	1.2×10^{-2}
Kazanjian and Stevens (1984)	Not known	–	$\frac{k_1 C_{\text{HF},0}}{1 + K_2 C_{\text{HF},0}}$	12	HF (0.05–1)	Not known
Miner et al. (1969)	Circular coupons	1.61	$kC_{\text{HNO}_3}^{-0.048} C_{\text{HF},0}^{-0.73}$	1–5	HF (0.01–0.13)	8.7×10^{-5}
Bray et al. (1986)	Not available	NA	$kC_{\text{HF},0}^{1.2}$		HF (0.05–0.2)	0.54–48.7

The computed activation energies and order of reaction are compared with those published in the article.

of plutonium tetrafluoride (Barney 1977, Kazanjian and Stevens 1984). Moreover, HF is corrosive to the process equipment and interferes in the solvent extraction steps of the reprocessing (Kazanjian and Stevens 1984). Several authors studied the kinetics of dissolution of PuO₂ with fluoride promoters. A brief summary is given below. The kinetic data analysis of PuO₂ in acid solutions is given in Table 3.

Barney (1977) proposed that the reaction on PuO₂ surface with the undissociated HF as the rate-controlling step. Moreover, it was also observed that HF makes strong complex with Pu(IV) to produce PuF_x^{4-x} complexes, and the dissolution rate decreases when the total concentration of Pu(IV) is greater than that of HF. Hence, it was concluded that HF is getting consumed in stoichiometric quantity as the reaction proceeds, and its role is beyond a catalyst in the process.

The analysis of IDR versus time data for a pellet (Uriate and Rainey 1965) indicates that IDR is proportional to the 4th power of HNO₃ concentration and the 1.31th power of HF concentration. On the other hand, Barney (1977) studied the dissolution of PuO₂ powder in HNO₃ and HF mixture. The experimental data were obtained in the kinetically controlled regime by eliminating the effect of stirring speed as a variable with the experiments performed above 400 rpm. The authors investigated the effects of surface area, HF and HNO₃ concentrations, and

temperature on the initial dissolution rate. The experimental results were then used for understanding the rate-controlling step and the estimate of overall rate of reaction. They observed that the initial rates are the same for several HNO₃ concentrations, and hence, HNO₃ was not considered in the rate-determining reaction step. Furthermore, they noticed that the measurement of fluoride on the PuO₂ surface during the dissolution indicates that some fraction of fluoride gets adsorbed on the surface, and it is not sensitive to the total HF concentration. Hence, it was postulated that the rate of reaction could be expressed as a function of non-complexed HF. The rate equation was given by $r = kC_{\text{HF}}$, where C_{HF} is the concentration of non-complexed HF. Under the assumption that the reaction proceeds uniformly over the surface where the particles are considered to be of identical size and shape, we computed the activation energy for the data of Barney (1977), which was 54.3 kJ mol⁻¹.

The value computed in the analysis is in line with that obtained by Barney (1977). The analysis of experimental data of Bray et al. (1986) and Miner et al. (1969) shows that the dissolution rate is proportional to the 1.2th and 0.73th powers of the initial concentration of HF, respectively. In the case of the study by Miner et al. (1969), it can be seen that the dissolution rate is around zeroth power of HNO₃ concentration, which is in line with the reasoning of Barney (1977). However, the activation energy value of

6.7 kJ mol⁻¹ reported by Miner et al. (1969) indicates the diffusion controlled process, which is exactly in contrast to the observation made by Barney (1977).

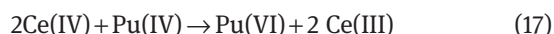
In contrast to the above authors, Kazanjian and Stevens (1984) found that the dissolution of PuO₂ increases when HF concentration was increased up to a certain concentration (0.2 M in their experiments). Above 0.2 M HF concentration, the dissolution rate decreases with further increase of HF concentration. Our analysis of Kazanjian and Stevens' (1984) data indicates that the behavior of the experimental data can be captured by a rate expression with an inhibiting term for the concentration range. The experimental data are used to compute the values of rate constant k_1 and the equilibrium constant K_2 for 0.05–0.5 M HF concentrations. The obtained values for k_1 and K_2 are 7.38×10^{-5} (m s⁻¹) and 3.5582 M⁻¹, respectively.

It should be noted that HF concentration is less than 0.2 M in the study of Barney (1977), Miner et al. (1969), Uriate and Rainey (1965), and Harmon (1975a,b). In this concentration range of HF, the dissolution rate is approximately the first order, as the inhibition term has negligible influence on the rate. However, above 0.2 M HF (or KF in case of Harmon 1975a,b), the inhibition term becomes significant, and hence, the dissolution rate decreases. Kazanjian and Stevens (1984) observed that PuF₄ started to precipitate in the solution above 0.2 M HF. Moreover, at 0.7 and 1 M HF concentrations, high amount of PuF₄ was found in the undissolved residue. This indicates that PuO₂ dissolves rapidly in the solution and immediately precipitates as PuF₄. Barney (1977) also observed the precipitation of PuF₄ when the total concentration of HF is greater than 0.1 M. However, they noted that PuF₄ re-dissolves again with time as more Pu is dissolved. Moreover, they also observed that PuF₂⁺² and PuF⁺³ complexes were present in significant quantities in the solution for the concentration of HNO₃ below 10 M.

As part of a study to systematically evaluate the dissolution behavior of several different actinide oxides, Berger (1990) utilized carbon paste electrochemical techniques and considered the following general dissolution mechanisms for PuO₂: (i) with no redox reaction, producing the Pu(IV) species in solution; (ii) by oxidation, producing either Pu(V) or Pu(VI); and (iii) by reduction, producing Pu(III). Although oxidative dissolution of PuO₂ is theoretically observed for the electrochemical electrode potentials above 1.43 V and 1.22 V, respectively, leading to the formation of Pu(V) and Pu(VI), only the reductive dissolution path was shown thermodynamically favorable in non-complex acidic media (Berger 1990, Madic et al. 1992).

3.2.4 PuO₂ dissolution in HNO₃-Ce(IV) solution

There has been a strong need to develop alternative methods to quantitatively dissolve PuO₂ rapidly without opting for any corrosive reagents like HF. Thus, redox chemistry becomes very prominent and led to many industrial improvements. Initially, Ce(IV) was used as a promoter to enhance the performance of HF-based processes for dissolving plutonium-rich scrap materials to recover plutonium (Uriate and Rainey 1965, Harmon 1975a,b, Horner et al. 1977). Berger (1990) experimentally determined the half-cell potential of Ce(IV)-Ce(III) couple, which paved way for more exploration of this method for the dissolution of plutonium-rich spent nuclear fuel. Harmon (1975a,b) noted that oxidization of Pu(IV) to Pu(VI) by Ce(IV) is given by the following mechanism:



Uriate and Rainey (1965) also studied the effect of addition of Ce(IV) on the dissolution rate. They added ceric ammonium nitrate as Ce(IV) source. They observed that the dissolution rate increased by the addition of Ce(IV) for the concentrations of HNO₃ solution less than 2 M. The rate was also found to be proportional to Ce(IV) concentration. However, for higher concentrations (>4 M) of HNO₃, the rates were found to be independent of Ce(IV). It was noted that the rate of reaction was still low for all practical applications. The analysis of the data shows that the dissolution rate is proportional to the 0.78th power of HNO₃ and the 0.58th power of Ce(IV) concentration.

It has been observed that the addition of Ce(IV) to HNO₃ increases IDR (Harmon 1975b, Horner et al. 1977). However, Harmon (1975b) observed that the dissolution rate increases with the concentration of Ce(IV) until 0.025 M in HNO₃-KF solution, while it decreases above 0.025 M concentration. This result is in contrast to that obtained by Horner et al. (1977). This phenomenon can be attributed to the ratio of KF to Ce(IV). It was observed that at the KF to Ce(IV) ratio of 1, the dissolution rate was less than that of either promoter alone (Harmon 1975b). Moreover, it was observed that mixed Ce(IV) and KF system at certain KF/Ce(IV) yielded better results than with either of the additives alone. This indicates the importance of ratio optimization for optimal dissolution rate. Moreover, the stoichiometric amount of Ce(IV) was needed for complete dissolution of PuO₂, which indicates that Ce(IV) does not behave as a catalyst in the process (Harmon 1975b). Hence, the higher concentration of Ce(IV) is required to dissolve high amount of PuO₂. It was shown that there was marginal effect of Ce(III) on the dissolution of PuO₂.

(Horner et al. 1977). Moreover, hydrothermal precipitation of CeO_2 under pressure and high temperature was observed during the experiments with low HNO_3 concentration (<2 M) (Harmon 1975b).

Using the experimental data of Horner et al. (1977), it was found that the dissolution rate was proportional to the first power of Ce(IV) concentration. The activation energy of 60 kJ mol^{-1} was computed from the dissolution rate versus temperature data. This result indicates that the intrinsic kinetics is the rate-controlling step, which is also the case for HNO_3 -HF system.

3.2.5 PuO_2 dissolution in HNO_3 with other additives

Various complexing agents, Ag(II)-Ag(I) and Co(III)-Co(II), etc., were added to oxidize Pu(IV) to Pu(VI) and, hence, preventing the formation of PuF_4 and enhancing the dissolution rate (Berger 1990, Ryan et al. 1990, Madic et al. 1992, Zawodzinski et al. 1993). Kazanjian and Stevens (1984) observed that several complexing agents enhanced the dissolution rate, particularly, Ce(IV) and Ag(II). The authors also observed that the dissolution was kinetically controlled.

Gelis et al. (2011) investigated Am(V)/Am(III) and Am(VI)/Am(III) couples as mediators of the oxidative dissolution of PuO_2 instead of foreign redox couples. Americium dioxocations were generated by ozonation of solutions containing Am(III). They found that Am(III) increases the dissolution rate, and it may be a promising alternative to the external additives.

With ozone as a complexing agent, Uriate and Rainey (1965) observed that there is a marginal increase in the dissolution rate. However, at high concentrations of HNO_3 , Ce(IV) and ozone were reduced rapidly due to their limited stability and, hence, were not available for catalyzing the reaction. They also used additives such as H_2O_2 , $\text{Na}_2\text{Cr}_2\text{O}_7$, NaNO_3 , and LiNO_3 . However, they found that there is no effect of these additives on the dissolution rates.

Bjorklund and Staritzky (1954), in their work on reactivity of PuO_2 , had already indicated the feasibility of this method using a mixture of hydrochloric acid and iodide. Berger (1990) estimated $\text{PuO}_2(\text{s})/\text{Pu(III)(aq)}$ couple's standard potential, which paved way for the studies on Cr(II)/Cr(III) couple in sulfuric acid media to be used for PuO_2 dissolution. The work of Shakila et al. (1987) in HCl media using Fe(II)/Fe(III) couple also demonstrated the feasibility of the reductive dissolution of PuO_2 . In this work, it was found that the dissolution took place vigorously as long as Fe(II) was available. Hence, hydrazine was used, which prolonged the availability of Fe(II) by reducing Fe(III) and thereby the dissolution reaction. Shakila et al. (1989) also reported the

improved dissolution in HNO_3 -HF medium in the presence of hydrazine. Fife (1996) carried out a detailed kinetic study of PuO_2 dissolution in HCl media using ferrous as electron transfer catalyst. They modelled the reaction using the classical non-porous shrinking spherical core model and found the dissolution to be kinetically controlled.

3.2.6 Effect of calcination temperature/surface area

The preparation of PuO_2 can affect its dissolution properties. Harmon (1975b) showed that the dissolution of PuO_2 decreases as the calcination temperature of PuO_2 increases. Etter and Herald (1974) investigated the effect of calcination temperature and the concentration of HF on the dissolution of PuO_2 . Their results indicated that the dissolution of PuO_2 decreased progressively as the calcination temperature increased. They suggested a calcination temperature of $500 \pm 50^\circ\text{C}$ for a complete decomposition of the oxalate and maintained a reasonable dissolution rate. Moreover, the high concentration of HF also helps to increase the dissolution of PuO_2 at the given calcined temperature. The surface area of PuO_2 particles per gram decreases as PuO_2 calcination temperature increases. This might also contribute to a decrease in the dissolution rate. Recently, CeO_2 has been used as a surrogate for UO_2 and mainly for PuO_2 in MOX (Kim et al. 2008). Particularly, the role of energetically reactive site such as surface defects, grain boundaries, and artefacts of CeO_2 pellet has been investigated on the initial dissolution rate (Corkhill et al. 2014, 2016). They noted that higher energetically reactive sites led to higher dissolution rate. These energetically reactive sites are of two kinds: (i) natural surface defect such as grain boundaries and (ii) surface defects induced during preparation. It has been noted that grain boundaries dissolve rapidly than do other sites in solids (Corkhill et al. 2014). Furthermore, the dissolution of facet formed during the oxide preparation was found to be instantaneous. They also found that a chemical defect such as elimination of oxygen vacancies had significant effect on the dissolution rate. Szenknect et al. (2012) investigated the microstructure effect on the dissolution of Ce(IV)-Ne(III) oxides. They observed that the more porous structure were formed after the initial surface dissolution.

3.3 Dissolution of thorium dioxide

3.3.1 Preamble

Thorium dioxide (ThO_2)-based fuel is important for the nuclear power using the breeder reactor concepts

(Hubert et al. 2001). The dissolution rate of ThO_2 is orders of magnitude more than uranium in HNO_3 under the identical conditions (Moore et al. 1957). On the other hand, similar to that of PuO_2 , the dissolution of ThO_2 in HNO_3 can be significantly enhanced by the addition of small amounts of HF (Takeuchi et al. 1971). In this section, the following aspects of the dissolution of thorium oxides are analyzed and reviewed: (i) reaction kinetics and mechanism, (ii) effect of stirring speed, (iii) role of surface area and pellet shapes, and (iv) role of calcination temperature.

3.3.2 Reaction kinetics and mechanisms

Moore et al. (1957) studied the effects of variables such as concentrations of HF and HNO_3 on the dissolution rates of thorium dioxide wafers and developed a quantitative model. To perform the experiments, the following reaction was considered:



It was observed that the dissolution rate increased linearly with HF concentration up to 0.1 M and decreased at higher concentrations. Above 0.1 M HF, they observed a white coating on the surface of the wafer. They postulated that the coating may be of thorium fluoride or calcium fluoride (impurity). Hence, the dissolution rate decreased at high concentrations due to precipitation of ThF, which is a similar phenomenon as the dissolution of PuO_2 . A kinetic expression for the dissolution rate obtained from

the experimental data is given in Table 4. The kinetic expression indicates that the rate is proportional to the 1.4th power of HNO_3 concentrations while the inhibition type of kinetic equation with respect to the HF concentration was employed.

Hyder and Prout (1966) studied the dissolution of ThO_2 particles and pellets in 10–16 M HNO_3 containing HF. They also observed the precipitation of ThF_4 in the solution for concentrations greater than the 0.1 M HF concentration. Furthermore, the dissolution rate increased up to 13 M HNO_3 concentration, and then it was observed to decrease upon increasing the HNO_3 concentrations. The kinetic expression obtained from the analysis is shown in Table 4. The results indicated the inhibition kinetics for HNO_3 concentrations.

Takeuchi et al. (1971) studied the dissolution of sintered ThO_2 circular disk in the HF- HNO_3 solutions at different temperatures and over a wide range of HF (0.005–0.035 M) and HNO_3 (2–6 M) concentrations. On the basis of the experimental observations, the authors proposed a mechanism for the dissolution reaction on the surface of ThO_2 disk. They observed the absence of surface products that can inhibit the reaction. Furthermore, the dissolution rates were found to increase with an increase in the HF concentration up to 0.035 M, and then, it started to decrease. This indicates an inhibition nature of reaction kinetics beyond that of a certain concentration. Similar observation was made for the undissociated HNO_3 concentrations. Based on the experiments, the following mechanism for the surface reaction was proposed (Takeuchi et al. 1971):

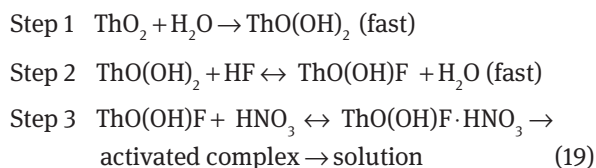
Table 4: Summary of results obtained via analysis of experimental data in the published literature for ThO_2 .

Authors	Shape	Activation energy (kJ mol ⁻¹)	Kinetic expression	Conc. HNO_3 (M)	Additive	Surface area (m ² g ⁻¹)
Moore et al. (1957)	Circular wafer	–	$k_0 \frac{K_1 C_{\text{HF}}}{1 + K_1 C_{\text{HF}}} C_{\text{HNO}_3}^{1.4}$	2–6.5	HF (0.0005–1)	9.62×10^{-6}
Hyder and Prout (1966)	Particle	–	$\frac{K_1 C_{\text{HNO}_3}}{1 + K_1 C_{\text{HNO}_3}}$	10–16	HF (0.05)	Not known
Takeuchi et al. (1971)	Circular disk	11.70	$k(E, T) \frac{K_1 C_{\text{HF}}}{1 + K_1 C_{\text{HF}}} \frac{K_2 C_{\text{HNO}_3}}{1 + K_2 C_{\text{HNO}_3}}$	2–6	HF (0.005–0.035)	6.07×10^{-5}
Shying et al. (1970)	Particles	13.45 ^a	–	1–13	HF (0.002)	3.55 ^b
Keshtkar and Abbasizadeh (2016)	Powder	21.3 (HNO_3) 6.8	–	3.5–9.5	HF (0.005)	–

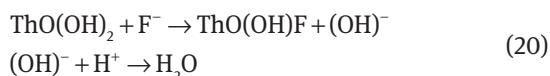
The computed activation energies and order of reaction are compared with those published in the article.

^aThe activation energy is computed using the initial rate versus time data at constant HNO_3 and HF concentration and varying temperature.

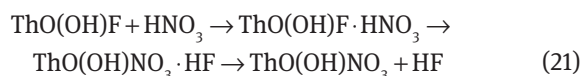
^bTotal surface area measured by the nitrogen adsorption method.



In step 1, the fast reaction between ThO_2 and water takes place to produce hydroxyl complex on the surface of ThO_2 . In step 2, HF concentration reacts with hydroxyl complex (which was assumed to cover fraction of total surface) to produce surface fluoride and water. In step 3, HNO_3 molecule adsorbs on the surface fluoride and produces the soluble activated complex. Here, it was assumed that a minor fraction of HF is dissociated. Hence, they concluded that the rate of dissolution is proportional to fraction of the surface covered by the undissociated HF and HNO_3 . Takeuchi et al. (1971) have reported the heat of activation energy to be 43.9 kJ mol^{-1} . Furthermore, the inhibition kinetic rate expression is also shown in Table 4. In their follow-up study, Takeuchi and Kawamura (1972) tried to identify the actual species in HF (F^- , HF^- , dissociated HF), which probably reacts with the hydroxyl surface of ThO_2 . It was concluded that fluoride ion (F^-) reacts with the hydroxyl surface, as follows:



The second step indicates that the liberated hydroxyl ion reacts with the hydrogen ions to form water. Hence, the equivalent amount of fluoride and hydrogen ions is consumed in the reaction of fluoride ions with the hydroxyl surface. Furthermore, they proposed that HF acts as a catalyst. As fluoride can form stronger hydrogen bond than hydroxyl, surface fluoride ion may act as a bridging site for HNO_3 . Hence, step 3 was modified, as follows:



Shying et al. (1972) also investigated the mechanism and kinetics of the dissolution of crystalline thoria particles in HNO_3 -HF system. Similar to the study by Takeuchi and Kawamura (1972), it was observed that fluoride ion adsorbs on hydroxyl charged positive surface of ThO_2 (Shying et al. 1972). In contrast to the other authors in Table 4, they claimed that fluoride sites as well as fluoride in solution are involved in the reaction mechanism. They postulated “Langmuir-Hinshelwood” type of reaction mechanism, as follows:

1. reaction between the oxide and water or protonated species to produce hydroxyl surface

2. dissociation of hydroxyl surface compounds to form a positively charged surface species
3. F^- adsorption
4. reaction of hydroxyl surface and fluoride ions with the fluorinated surface sites
5. desorption of a thorium fluoride complex

The proposed mechanism of Shying et al. (1972) is similar to that of Takeuchi and Kawamura (1972). Furthermore, they proposed an expression for the dissolution rate that is proportional to the activities of fluoride in solution (order 1) and protons (order 2) and the concentration of adsorbed fluoride on ThO_2 surface. The computed activation energy using the initial rate method at different temperatures is 13.45 (reported value 18) kcal mol^{-1} . This value is higher than the one obtained by Takeuchi and Kawamura (1972).

3.3.3 Effect of stirring speed

Hyder and Prout (1966) observed that mild agitation at boiling point of HNO_3 increased considerably the dissolution rate. Furthermore, in studies of Shying et al. (1972) and Takeuchi and Kawamura (1972), the bulk solution diffusion was eliminated as a rate-controlling step. Shying et al. (1972) observed that the increase in the agitation speed from low to rapid did not increase the dissolution rate significantly. Takeuchi and Kawamura (1972) observed that the dissolution rate did not depend on the stirring speed from 250 rpm to 1000 rpm. In both studies, the authors took adequate care to eliminate contribution of mass transfer in the bulk and performed experiments in the kinetically controlled regime.

3.3.4 Effect of surface area and shape

Table 4 indicates that the activation energies vary with the shape of particles. Furthermore, the reported values by the authors vary considerably [$10.5 \text{ kcal mol}^{-1}$ for Takeuchi and Kawamura (1972) and 20 kcal mol^{-1} for Shying et al. (1970)] with the shapes. Hyder and Prout (1966) observed that the dissolution rates depended on the particle sizes. In their experiments, they found that fine particles dissolved rapidly in comparison to large particles. It has been concluded that the effective surface area is essential for computing the correct dissolution rates in other oxides, and hence, it is important to measure the effective surface area for ThO_2 . Furthermore, ThO_2 pellets have been dissolved to study the effect of microstructure on the dissolution UO_2 in fuel matrix (Myllykylä et al. 2015) in the diluted

HNO_3 . They observed that surface defects have an effect on the local dissolution rates.

4 Dissolution of MOX

4.1 Preamble

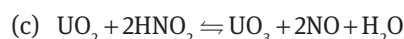
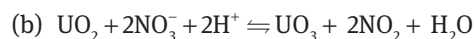
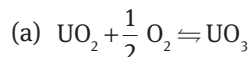
MOX fuel of urania, thoria, and plutonia is typically used to drive FBRs. The plutonium composition in the MOX fuel varies from about 10% by weight to about 30% by weight. If plutonium exceeds this amount, it renders the fuel practically insoluble in highly concentrated nitric acid medium (Uriate and Rainey 1965). Most of the literature articles on MOX dissolution were a result of investigation of the MOX fuel leaching characteristics during the long-term storage of spent MOX fuel from environmental safety point of view (Forsyth and Werme 1992, Serrano et al. 1998, Jégou et al. 2010, Claparede et al. 2011b, Poinssot et al. 2012a). Furthermore, these studies have also investigated the roles of physicochemical parameters and addition of actinides in MOX dissolution. Next, we will analyze these works to understand the dissolution of MOXs (or surrogate oxides) in nitric acid.

4.2 Reaction kinetics and mechanism

First detailed work on the dissolution of (U, Pu) MOX fuel was done by Uriate and Rainey (1965). They have studied the dissolution behavior of both unirradiated and irradiated MOX with 20% PuO_2 and rest UO_2 by weight. They have attributed to the sluggish kinetics of MOX fuel in nitric acid predominantly to the fuel fabrication methodology and its process conditions. MOX fuel fabricated through co-precipitation route has much faster dissolution kinetics compared to those fabricated through powder metallurgy methods. Also, they have observed that co-precipitated fuel goes to dissolution completely as against the MOX obtained by powder blending route. They have also found that process conditions like sintering temperature and time influence their dissolution kinetics to a greater extent. They have also found out that under the experimental conditions of their work, irradiated MOX fuel was found dissolved about five times faster than their unirradiated counterpart. They have estimated the initial dissolution rates of the abovementioned unirradiated and irradiated MOX fuel in nitric acid to be about $1 \text{ mg cm}^{-2} \text{ min}^{-1}$ and $3 \text{ mg cm}^{-2} \text{ min}^{-1}$, respectively.

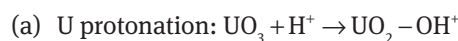
Heisbourg et al. (2003) dissolved Th and U MOX powder to study dissolution rate of individual metal. They proposed a mechanism of MOXs dissolution in three steps as follows:

1. Oxidation of U at the surface via following reactions:

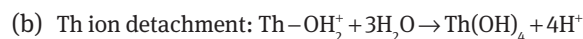


They pointed out that reaction (a) is more likely to occur at low concentration ranges than do other reactions based on the reduction potential values of the species. Note that reaction (c) cannot happen at 6–10 M HNO_3 concentrations due to the short life of HNO_2 at high concentrations of HNO_3 . Hence, at high concentrations of HNO_3 , the oxidation of U takes place through reaction (b).

2. Fast protonation of Th and U from the surface layer



3. Detachment of the metal ions



Furthermore, it can be observed that Table 5 indicates the preponderant role of Th and U in MOXs in dissolution (Heisbourg et al. 2003, 2004). When Th is preponderant, the dissolution of U is a weak function of the nitric acid concentrations; order of reaction is less than one. On the other hand, when U is preponderant, the dissolution of U is a strong function of the HNO_3 concentrations (>1) and behaviors similarly to the dissolution of uranium oxides. They also observed that $\text{ThO}_n(\text{OH})_{4-2n} \cdot \text{H}_2\text{O}$ precipitates formed on the surface of solid at $\text{pH} > 2$ and slowed down the uranium dissolution (Heisbourg et al. 2004). Hence, the dissolution process of U is then more governed by the diffusion process through the thorium precipitate layers, and it is diffusion controlled (Heisbourg et al. 2004). Furthermore, it can be observed from Table 5 that the activation energy decreases with the increase of U contained in the MOX.

Hubert et al. (2008) studied the dissolution of Th and Pu oxide in weak nitric and hydrochloric acids. They observed that the species Th^{4+} is the predominant form in aqueous solution at $\text{pH} < 2$ while ThOH^{3+} is predominant for $\text{pH} > 2$. On the other hand, Pu^{4+} and PuNO_3^{3+} exist along with hydrolyzed Pu species at $\text{pH} < 2$. At $\text{pH} > 2$,

Table 5: Summary of results obtained via analysis of experimental data in the published literature for MOXs-I.

Authors	HNO ₃ conc. range (M)	Shape/temperature range (°C)	Composition	Order of reaction	Activation energy (kJ mol ⁻¹)
Heisbourg et al. (2003)	0.01–5	Powder	Th _{0.76} U _{0.24} O ₂	0.76	31.96
			Th	0.64	
			U		
			Th _{0.63} U _{0.37} O ₂	0.83	
			U	0.83	
Heisbourg et al. (2004)	10 ⁻⁴ –10 ⁻¹	Powder	Th _{0.47} U _{0.53} O ₂	1.31	15.41
			U in Th _{0.47} U _{0.53} O ₂	1.23	
			U in Th _{0.33} U _{0.67} O ₂	0.89	
			U in Th _{0.19} U _{0.81} O ₂	0.173	
			ThO ₂	0.55	
Hubert et al. (2008)	10 ⁻³ –1	Powder	Th _{0.87} Pu _{0.13} O ₂		97.74
			Th	0.77	
Horlait et al. (2012)	0.01–4	Powder/5–90	Nd	0.47	100.78
			Th _{0.58} Nd _{0.42} O ₂		
			Th _{0.90} Nd _{0.10} O ₂		
			Th _{0.81} Ce _{0.19} O ₂		
			Th	0.50	
Claparede et al. (2011a)	0.1–6	Powder	Ce _{0.91} Nd _{0.09} O ₂	1.07	55.6
			Ce	1.04	
Claparede et al. (2011b)	0.1–6	Powder	Nd	1.04	55.6
			CeO ₂	0.61	

The average computed activation energies and order of reaction are presented.

Pu(OH)₃⁺, Pu³⁺, and Pu(NO₃)₂⁺ are present in the solution. Furthermore, the order of reaction with respect to HNO₃ concentrations is improved in MOXs in comparison to the thorium oxide.

Recently, the role of physicochemical parameters such as temperature, acidity, and microstructure has been investigated in the dissolution of Th-U MOX and its surrogates (Horlait et al. 2014, Claparede et al. 2015, Corkhill et al. 2016). Claparede et al. (2015) studied kinetics of Th_{1-x}U_xO₂ (x = 0.16, 0.52, 0.75) and Th_{0.81}Ce_{0.19}O₂ pellets in 0.1–6 M nitric acid. It can be observed that the preponderant Th in oxides leads to higher activation energy (average of 50 kJ mol⁻¹) and less dependent on HNO₃ concentration with n = 0.50–0.74. This indicates that surface reaction controlled the phenomena (Claparede et al. 2015). On the other hand, the dissolution of the oxides with the preponderant U is similar to that of the uranium oxide. It can be observed that the order of reaction for HNO₃ is similar to that for the UO₂ dissolution, the average order of reaction n = 1.5. This was attributed to two successive chemical reactions: fast oxidation of U⁴⁺ to U⁶⁺ and the detachment of activated complexes of U⁶⁺. These reactions are a subset of the reactions proposed by Heisbourg et al. (2004).

Recently, it has been considered to recycle minor actinides (rare-earth elements produced during fission) with MOX for the next-generation fuel (Szenknect et al. 2012, Tocino et al. 2014). Several studies have been published on synthesis of rare-earth doped mixed oxides (REMOX) and the effect of various physicochemical parameters on the dissolution of REMOX (Horlait et al. 2012, 2014, Tocino et al. 2014, Baena et al. 2015). Furthermore, the incorporation of rare-earth also induces oxygen vacancies (Baena et al. 2015), and hence, the role of trivalent lanthanide incorporation rate has been also investigated (Horlait et al. 2012, Tocino et al. 2014). Horlait et al. (2012) studied the dissolution of Th_{1-x}Nd_xO_{2-x/2} and the effect of solid composition and temperature of the dissolution. It has been observed that the incorporation of Nd enhanced the dissolution rate of oxides in comparison to thorium oxides. The enhancement of dissolution can be attributed to weaken crystal lattice due to incorporation of Nd³⁺. Furthermore, the order of reaction with respect to HNO₃ concentration has similar magnitude as those obtained by Claparede et al. (2015) and Tocino et al. (2014) (see values in Tables 5 and 6), and it indicates that the surface reaction controlled mechanism is present. This also can be confirmed by the activation energy of the reaction, which

Table 6: Summary of results obtained via analysis of experimental data in the published literature for MOXs-II.

Authors	HNO ₃ conc. range (M)	Shape/temperature range (°C)	Composition	Order of reaction	Activation energy (kJ mol ⁻¹)
Tocino et al. (2014)	0.01–4	Pellet	U _{0.75} Th _{0.25} O ₂	1.71	
	0.5–4		U _{0.75} Ce _{0.25} O ₂	2.15	
	0.01–0.5			1.65	
	0.01–4		U _{0.75} Nd _{0.25} O _{1.875}	1.04	
	0.5–4			1.4	
	0.01–4		U _{0.75} Ge _{0.25} O _{1.875}	0.99	
	0.5–4			1.47	
	0.01–4		Th _{0.75} Nd _{0.25} O _{1.875}	0.62	
	0.01–4		Ce _{0.75} Nd _{0.25} O _{1.875}	0.74	
	Claparede et al. (2015)		0.1–6	Pellet/40–90	Th _{0.76} U _{0.24} O ₂
		Th	0.74		54.43
		U	0.52		48.45
0.1–4		Th _{0.48} U _{0.52} O ₂			
		Th	1.53		22.2
		U	1.67		18.88
0.1–4		Th _{0.25} U _{0.75} O ₂			
		Th	1.24		24.16
		U	1.29		23.01
0.1–6		Th _{0.81} Ce _{0.19} O ₂			
		Th	0.52		61.05
		Ce	0.50		54.3

The average computed activation energies and order of reaction are presented.

is greater than 20 kJ mol⁻¹. Furthermore, the activation energy of the dissolution is independent of composition of lanthanide. Tocino et al. (2014) investigated the role of oxygen vacancies caused by the incorporation of lanthanides on the dissolution kinetics. It can be observed from Table 6 that the order of reaction of the U dissolution rate in MOX is similar to that of UO₂ for 0.5–4 M HNO₃, i.e. the oxygen vacancies do not play any role in dissolution rates. Furthermore, the dissolution rate of Th and Ce with respect to the HNO₃ concentrations (Tocino et al. 2014) (see Table 6) is similar to the one obtained by Horlait et al. (2012, 2014) (see Table 5). Furthermore, it can be seen that oxygen vacancies affect the dissolution rate for 0.01–0.5 M concentration range. Also, the incorporation of Ce and Th did not change the dissolution rate of U in MOX at higher concentrations. However, at concentrations <0.5 M, the dissolution rate of U decreased in case of U_{0.75}Ce_{0.25}O₂. This was attributed to a different dissolution mechanism that could be due to the small amount of U⁵⁺ and Ce³⁺ (Tocino et al. 2014). Based on the observations in Table 6, it can be concluded that the redox reactions mechanism plays an important role at higher concentrations of HNO₃, while the oxygen vacancies play a role at lower concentrations. Furthermore, it can be noted that the incorporation of lanthanide reduces the activation energy (Tocino et al. 2014) but still greater than 20 kJ mol⁻¹, and hence, it suggests

that the surface reaction controlled mechanism presents dissolution.

4.3 Effect of incorporation of Fission Products

Mixed actinide oxides are a potential nuclear fuel for gen IV nuclear reactors like sodium cooled fast reactors (SFR) and gas cooled fast reactors (GFR) (Horlait et al. 2014). These reactors are conceptualized to recycle the minor actinides produced during irradiation for their long-term safe deployment. Often Ce(IV) and Nd(III) have been used as the surrogate to study the behavior of actinides(IV) and lanthanides(III), respectively, during various nuclear fuel cycle operations. Hence, the chemical durability of Ce_{1-x}Nd_xO_{2-x/2} as a surrogate of nuclear fuel under various reprocessing conditions gained importance in the framework of the development of Gen IV reactor concept. The corrosion resistance of these surrogate MOX fuels was recently reported (Claparede et al. 2011a, Horlait et al. 2012). These studies highlighted the influence of the physicochemical properties such as crystallite size, specific surface area, and porosity on the normalized dissolution rates under various conditions (temperature, nitric acid concentration) on their dissolution rates. The

incorporation of Nd(III) in place of tetravalent actinide oxide lattice, which is also one of the Fission products (FPs), creates oxygen vacancies in the solid structure for the charge compensation. This would lead to structural changes in the solid, thereby weakening the crystal lattice affecting its dissolution rate (Horlait et al. 2011, 2012). Among all the physicochemical properties, this weakening of the lattice was found to be the predominant contributor for the change in the dissolution rate (Horlait et al. 2012). When the effect of temperature was studied to determine the apparent activation energy of dissolution of $\text{Th}_{1-x}\text{Ln}_x\text{O}_{2-x/2}$ mixed oxides, the values were found to be around 95 kJ mol^{-1} , which was much higher than that of ThO_2 under similar conditions (20 kJ mol^{-1} in Heisbourg et al. 2003). This indicates the strong influence of incorporating the trivalent lanthanide into the crystal lattice on the dissolution rate. The studies on the effect of nitric acid concentration also revealed the fact that the dissolution reaction is more likely controlled by surface processes involving the formation of activated complexes. It was also found that these structural changes also would lead to the rearrangement of metal atoms within the fuel matrix, which would generate compositional heterogeneity within the pellet and thus would affect their dissolution rates as well, especially due to the generation of volatile FPs and their subsequent diffusion within the fuel matrix (Shirsat et al. 2009). Simulated studies have also indicated that as the nuclear fuel undergoes irradiation, more FPs get generated, which imparts more disorderliness within the solid structure (Tahara et al. 2011). On the contrary, irradiation leads to expansion of the crystal lattice. The effect of irradiation would be more pronounced when more FPs atoms are present in the lattice, which happens only at high burn up.

4.4 Effect of fission products and irradiation on dissolution kinetics

There have been some recent studies that indicate the effect of FPs on the dissolution behavior of thin film UO_2 and its simulant fuel samples in water before and after irradiation (Popel et al. 2017). These studies indicated that there is considerable increase in the dissolution rate initially in the non-radioactive fission product doped and irradiated samples, but gradually, the rate steadies down to that of an unirradiated sample. This was attributed to the structural changes within the solid fuel matrix due to the doping of FP atoms whose sizes and valencies are much different from actinides and the subsequent propagation of these structural defects on irradiation (Popel

et al. 2018). All of these kinds of studies reported so far in the literature were from the point of view of long-term stability of spent fuel under geological repository storage conditions. Although a similar trend is expected qualitatively for the dissolution of spent nuclear fuel under typical PUREX process conditions during reprocessing as well, more quantitative understanding is required for improving the safety, longevity, and efficiency of nuclear reprocessing facilities. Hence, more such systematic studies are to be carried out under typical PUREX process conditions. Presence of soluble FPs in the actinide oxide fuel matrix, especially UO_2 , has been shown to retard the solid-state oxidation of U(IV) to U(VI), which in turn is expected to retard the dissolution rate of UO_2 subsequently (Hanson 1998). Hence, some studies were undertaken to understand these effects by dissolving gadolinia-doped UO_2 in alkaline medium to evaluate the stability of the fuel under geological storage conditions. The results indicate the reduction in the dissolution rate considerably, especially at higher temperatures (up to 75°C) (Casella et al. 2016). But similar studies are required to be carried out systematically under PUREX process conditions for improving the design of a commercial spent fuel dissolution system.

5 Other modes of dissolution

Reflux heating in the nitric acid medium is the most preferred mode of dissolution of spent nuclear fuel as it is a simple method involving equipment whose designs are well understood. However, there are many other methods that have been used for dissolving nuclear fuel either from R&D point of view or from any specific/special-purpose point of view. Some of these methods are briefly discussed in this section.

5.1 Chemical dissolution using reagents other than nitric acid

As explained already in this work, uranium oxide dissolves comparatively faster than its plutonium and thorium counterparts. Hence, in the MOX containing UO_2 and PuO_2 or ThO_2 , UO_2 dissolves in the acid rapidly. However, other counterparts (PuO_2 or ThO_2) do not dissolve easily, and the undissolved residues will be rich in Pu or Th. One common mode of dissolving these undissolved residues is to heat them in concentrated nitric acid in the presence of strong complexing agents such as

HF, Ce(III), etc. (Heisbourg et al. 2003). Generally, these undissolved residues from the main dissolver vessel will be removed and treated with a strong complexing agent in a specially designed vessel called the super dissolver (Schiefelbein and Lerch 1971). The material of construction of this super dissolver is chosen to withstand the strong corrosive chemical environment during the dissolution of the residues. Hence, this method is not employed for regular processing. Generally, they are adopted whenever any Pu-rich scrap material has to be dissolved for their processing or disposal prior to which the Pu in them has to be recovered. Whenever the cladding material of the fuel used is Zr and Al alloys, medium other than nitric acid is proposed primarily to dissolve the clad for exposing the fuel to the dissolver for their dissolution. This is called the chemical decladding method. Some of such methods are DAREX (De Regge et al. 1980), which uses aqua regia; ZIRFLEX (Smith 1960), which uses ammonium fluoride-ammonium nitrate mixture; and SULFEX (Fisher 1960), which uses sulfuric acid.

5.2 Electrochemical

For the PHWR-type spent fuel where Pu content is very less (typically less than 0.4 wt%), dissolution can be carried out just by reflux heating in nitric acid medium. But when the Pu levels in the spent fuel increases, like about 30% or so in FBRs, just heating in nitric acid medium does not dissolve them completely. Some Pu-rich residues are always found. Hence, for such type of fuels, electrolytic dissolution was proposed as an alternate to dissolve the Pu-rich spent fuel completely in nitric acid medium (Fisher 1960). There was also another process proposed in which cerium was used to electrolytically catalyze the dissolution of PuO_2 (Cooley 1971). The method was primarily developed to avoid use of HF while processing Pu-rich spent nuclear fuel. It was claimed that cerium added in the process can be electrochemically regenerated, which helped in reducing its requirement to a really less amount. However, later, it was found that the major disadvantages of the process are the consumption of cerium in various other side reactions during dissolution (Harmon 1975a). Subsequently, considering the engineering difficulties in setting up an electrolytic cell inside a highly radioactive environment and their long-term routine operation, not much work was carried out in the electrolytic dissolution of spent fuel although many refractory scrap materials were processed by this method to recover the small amount of plutonium present in them.

5.3 Ultrasound

For the Pu-rich MOX of pure PuO_2 , which is difficult to dissolve completely in nitric acid medium alone, ultrasound-assisted dissolution may improve the dissolution kinetics. Hence, studies were initiated to dissolve refractory oxides like CeO_2 and PuO_2 by sonochemistry (Sinkov and Lumetta 2006a). The initial studies aimed at producing free radicals generated by cavitation (bubble implosion) to obtain either the oxidative or reducing conditions required for PuO_2 dissolution. The results though indicated that the dissolution rates were even less than employing reagents like Ag(II) and HF. Later, more work was carried out to test the effect of ultrasound on the dissolution of high fired PuO_2 (Juillet et al. 1997b). Overall, the results indicate that applying ultrasound for the dissolution of refractory PuO_2 does not offer any substantial advantage over the conventional “heat and mix” treatment.

A concise and complete account of the potential applications of sonochemistry in the spent nuclear fuel reprocessing operations has been given recently by Nikitenko et al. (2010), Sinkov and Lumetta (2006b), and Thompson and Doraiswamy (1999). Many previous studies have shown the advantages of ultrasound to over activate the surface of solids (Mason et al. 1996, Moisy et al. 1996, Thompson and Doraiswamy 1999). The intensification of mass transfer near the solid-liquid interface and the erosion of solids under ultrasound are explained by the asymmetric collapse of cavitation bubbles, which leads to micro jet impact at the solid surface (Mason et al. 1996).

A promising example of sonochemical dissolution was reported for metallic plutonium in HNO_3 -HCOOH mixture (Moisy et al. 1996). Dissolution of plutonium metal in HNO_3 medium is an important process for the preparation of MOX nuclear fuel and plutonium reference solutions (Polyakov et al. 1995). Plutonium metal is known to dissolve very slowly in HNO_3 at any concentration because of passivation (Cleveland 1970). It was reported that plutonium and Pu-Ga alloys could be dissolved in HNO_3 -HCOOH mixtures. In a 3.5 M HNO_3 -3 M HCOOH mixture at ambient temperature, the dissolution rate under mechanical stirring was found to be 100–200 $\text{mg min}^{-1} \text{cm}^{-2}$. However, under these conditions, potentially explosive denitration may occur during dissolution. This troublesome effect of denitration is not observed in more dilute HNO_3 , but the rate of metal dissolution also decreases considerably at a lower concentration of HNO_3 . Moreover, significant amount of insoluble sludge was formed after dissolution under these conditions. It was found that plutonium dissolution rate in 0.5 M HNO_3 -1 M HCOOH mixture is dramatically accelerated under the effect of 20 kHz ultrasound. Explosive

denitration does not occur at such concentrations of acids even under strong heating. A kinetic study revealed 24-fold acceleration of dissolution at the relatively low ultrasonic intensity of 1 W cm^{-2} at room temperature. Therefore, ultrasonic treatment provides not only a safe dissolution process but also significant enhancement of the dissolution rate. Furthermore, it was found that the fresh insoluble residue after plutonium dissolution ($\sim 5\%$) could be dissolved sonochemically by increasing the ultrasonic intensity and concentration of HNO_3 . Sludge dissolution is accompanied by oxidation of Pu^{3+} to Pu^{4+} , probably due to the reaction with HNO_2 . It was concluded that the mechanism of sonochemical plutonium metal dissolution is related to the intensification of mass transfer at the metal-solution interface, caused by acoustic cavitation and removal of passivating film from plutonium surface owing to the surface erosion induced by bubble asymmetric implosions. Dissolution of PuO_2 is another notoriously difficult but important process in nuclear fuel recycling. Until the 1980s, the primary method for dissolving PuO_2 was based on the long boiling of the oxide in HNO_3 -HF mixture under reflux condition. Such a method suffers from two main drawbacks: (i) the reaction is very slow, especially for high-temperature fired oxides with low specific area, and (ii) highly corrosive solutions are generated owing to the presence of fluoride ions, which raises the problems of safe effluent management. As PuO_2 could also dissolve in aqueous solutions as oxidized or reduced forms, i.e. as Pu(VI) and Pu(III) , respectively, new concepts based on redox reactions were developed subsequently.

At present, the best industrial process is consistent with the use of electrogenerated Ag^{2+} ions, which induce an oxidative dissolution of PuO_2 in HNO_3 medium (Bourges et al. 1986). Unfortunately, such a process is not very efficient for treating PuO_2 -bearing organic waste. This drawback has been overcome by using reducing species (Cr^{2+} , Ti^{3+}) in non-oxidizing acidic media like H_2SO_4 or HCl (Machuron-Mandard and Madic 1994). However, these acids are not compatible with the PUREX process. The effect of ultrasound at 20, 500, and 1700 kHz on the dissolution of CeO_2 and PuO_2 in 4 M HNO_3 solutions was studied (Juillet et al. 1997a). Cerium oxide was used as a non-radioactive surrogate for PuO_2 (Marra 2001, Kim et al. 2008). The authors observed a strong reduction of the particle grain size at 20 kHz, which did not take place at 500 kHz but appeared again, to a smaller extent, at 1700 kHz. At low frequency, the initial dissolution kinetics was accelerated only to about three to four times as compared to dissolution under mechanical stirring. At high-frequency ultrasound, the effect on the dissolution rate was even weaker than that at 20 kHz. The strongest effect

of ultrasound (15-fold acceleration) was observed in 1–4 M HCOOH solutions at the frequency of 1700 kHz. This result was attributed to the reductive dissolution of PuO_2 with the species formed after formic acid sonolysis. Hence, studies were initiated to dissolve refractory oxides like CeO_2 and PuO_2 by Thompson and Doraiswamy (1999). The initial studies were aimed at producing free radicals generated by cavitation (bubble implosion) to obtain either the oxidative or reducing conditions required for PuO_2 dissolution. The results though indicated that the dissolution rates were even less than those when employing reagents like Ag^{2+} and HF. Later, more work was carried out to test the effect of ultrasound on the dissolution of high fired PuO_2 . Overall, the results indicate that applying ultrasound for the dissolution of refractory PuO_2 does not offer any substantial advantage over the conventional, heat and mix, treatment (Beaudoux et al. 2015). Also some of the studies indicate that complete dissolution is not possible in the ultrasound-aided process due to the passivation phenomena, which decrease the rate (Viroit et al. 2012, 2013). A recent study also shows that although ultrasound-aided dissolution may not increase the rate of PuO_2 like refractory oxides, it does help in carrying out the dissolution process in comparatively milder conditions, which would auger well for the subsequent nuclear waste management unit operations (Beaudoux et al. 2015).

5.4 Photochemical

Some researchers have studied the photochemical dissolution of UO_2 powders and pellets in nitric acid medium in an effort to develop an alternate method for dissolution in milder conditions like low concentration nitric acid and ambient temperature. Based on their studies, Wada et al. (1996) initially proposed that in the photochemical aided dissolution of UO_2 , the nitrate ions present in nitric acid gets excited by absorbing the photochemical radiation whose redox potential is much higher than the unexcited one. This leads to faster dissolution rate than that in the dark condition. The work of Sasaki et al. (1998) further emphasized these findings. Later on, during further probing, Eung-Ho et al. (2000) came up with a more elaborate mechanism for the photochemical dissolution of UO_2 in nitric acid. They summed up their findings as follows.

1. Photochemical conditions certainly increase the rate of dissolution of sintered UO_2 pellets in nitric acid than in dark conditions.
2. Compared to sintered pellets, sintered particles dissolve much faster due to the increased surface area.

3. Presence of other elements such as Cs, Sr, Zr, Mo, Ru, and Nd increases the rate of photochemical dissolution further.
4. The increased rate is due to the NO_2 radical and nitrite ions that are generated and not due to the excited nitrate ions, as suggested by Wada et al. (1996).

However, considering the engineering challenges involved in the setting up these photochemical set up inside radioactive hot cells, and the chemical and radiation resistance of all the components involved in this set up, further studies on photochemical dissolution of nuclear materials were not pursued. Moreover, the presence of plutonium in the actual spent fuel will complicate the photochemical dissolution process further.

6 Suggestions for future work

The ultimate goal of this study is to estimate overall rate of reaction (combination of mass transfer and chemical reaction) at any point in the dissolver depending upon the concentration of nitric acid, nitrous acid, and particle characteristics (size and shape distribution, contact area, etc.). Secondly, the process model can be used for model-based monitoring, control, and optimization of dissolution processes. As mentioned in the introduction, the objective of this study is to reconcile and find shortfalls in the existing literature with respect to kinetic and transport model development. In this section, we will make suggestions regarding future experimental and modeling directions. The overall objective is to understand completely the intrinsic kinetics and the mass transfer characteristics. The following are the suggestions for future work:

1. Dissolution mechanism and kinetics: Understanding dissolution mechanism and kinetics of various oxides is important for improving the existing processes and designing industrial reactor. The following aspects need to be considered
 - Role of HNO_2 : It has been established in existing literature that HNO_2 plays an important role in the dissolution, particularly, of uranium oxides and at low rpm. However, exact role and mechanism of HNO_2 participation are still not clear. Hence, it needs to be studied.
 - Role of additives: Mechanistic studies of PuO_2 , ThO_2 , and MOXs dissolution in HNO_3 with various additives: HF (or KF), Ce(IV) or Am(III), etc. are considered to be effective rapid dissolution

of oxides. Detailed kinetic model and reaction mechanisms in presence of additive(s) need to be investigated. The roles of fluoride complexes can help not only to understand the mechanism of dissolution in presence of F ions but also to develop a detailed kinetic model. Hence, the exact mechanism of fluoride, intermediate complexes, and PuO_2 needs to be investigated by carefully designing experiments. Moreover, some results indicate the inhibition effect of HF in the dissolution process. Experiments with wide range of HF concentrations should be performed, which would ratify the observation in dissolution of PuO_2 . Furthermore, additives such as Ce(IV), Ag(II), and Co(II) might be useful additives for replacing corrosive fluorides. Hence, the experimental data on the dissolution with these additives need to be collected for their suitability. Furthermore, these experiments should be performed for understanding mechanisms and kinetics.

2. Mass-transfer phenomena: No information on mass-transfer rates and corresponding coefficients is available. The experimental studies indicated that the stirring speed plays an important role in the dissolution rate. Therefore, it is desirable to make measurements of mass-transfer coefficient in all types of batch and continuous dissolver. In such measurements, it is important that the same system of oxides-nitric acid be used. For this purpose, the knowledge of intrinsic kinetics developed in suggestion (1) would be useful. The procedure would consist of the measurement of overall rate of reaction comprising mass transfer as well as reaction steps. From this overall rate of reaction, the intrinsic rate of reaction can be subtracted for getting the value of mass transfer coefficient (k_L). Furthermore, it is desirable to get the value of k_L over a range of temperature of interest in the practice.
3. Role of surface area: The effective surface area is an important variable in the computation of IDR. In the case of UO_2 dissolution, the effective surface area changes with the progress of dissolution. This can affect the dissolution rate. Hence, the effective surface area and its change with the progress of dissolution need to be measured in future experiments and need to be incorporated in the dissolution rate expression. Furthermore, it has been observed that the calcination temperature maintained during fabrication affects effective surface area, surface state, and size of aggregates for Pu, Th, and MOXs. This information

needs to be included in overall rate expression. Therefore, experimental data need to be collected for the quantitative understanding of the effect of calcination temperature.

4. **Effect of additives:** As UO_2 dissolves rapidly compared to all other actinides oxides (used a nuclear fuel) in nitric acid, there has never been any necessity for an additive to alter the rate of its dissolution. Nevertheless, there have been many studies in the literature reporting the autocatalytic role nitrous acid, which aids the oxidative dissolution of UO_2 in nitric acid medium (refer to section 3.1 of this article for more details). On the contrary, nitrous acid is not expected to influence the dissolution rate of neither plutonia nor thoria as both plutonium and thorium remain in their most stable tetravalent state both in the solid and aqueous phases. But as urania is the major component of MOX nuclear fuels (both for PHWR and FBR), as nitrous acid accelerates the dissolution of UO_2 preferentially from the MOX fuel matrix, it renders the fuel more porous and increases its specific surface area, which leads to exposing more of the other components of MOX fuel ($\text{PuO}_2/\text{ThO}_2$ as the case may be) to nitric acid. This would result in an enhanced rate of the overall dissolution of the MOX fuel. This qualitative understanding of the behavior of MOX fuel in presence of an oxidizing additive like nitrous acid needs to be studied quantitatively. On the other hand, when it comes to the dissolution of plutonia and thoria in nitric acid medium, they invariably require some additives like HF, Ce(IV), Ag(II) etc., irrespective of other conditions. Although many such studies have been reported in the literature (refer to section 3.2 for more details), there is a dearth of quantitative information that is required for designing a commercial dissolution system for FBR and AHWR (advanced heavy water reactor) spent fuel reprocessing. Therefore, experiments have to be planned and carried out systematically under various conditions within the domain of PUREX process to unravel the effect of different potential additives on MOX fuel dissolution rate.
5. **Physicochemical parameters:** Physicochemical parameters are important in determining dissolution rates of oxides. Effect of dissolution temperature, pH, and complexing agents have been discussed in suggestion 1. In addition to these physicochemical parameters, it has been observed that structural properties of solid oxides (crystal defects, oxygen vacancies etc.), pellet density, grain structure and size, etc. have an effect on the dissolution rates (Claparede et al. 2011b, Horlait et al. 2011, Horlait et al. 2014, Tocino et al. 2014). These studies have been performed at low to medium HNO_3 concentrations from long-term storage of spent fuel viewpoint. Hence, the effects of these physicochemical parameters have to be studied at higher concentrations of HNO_3 relevant to reprocessing. Furthermore, experimental data should be collected to incorporate their effects for quantitative predictions in the dissolution rate models.
6. **Lanthanides doped oxides:** There are several studies to understand the dissolution rate of lanthanide doped oxides in the literature from long-term storage view point. However, there are no dissolution studies at nuclear reprocessing plant conditions. It is indeed important to investigate dissolution rates of lanthanides doped oxides at this concentrations as well.
7. **Continuous dissolver design:**
 - (a) In commercial practice, both batch and continuous dissolvers are in operation (Odom 1972, Carnal et al. 1989, Chatterjee and Joshi 2008, Sano et al. 2011). The batch category includes (a) stirred dissolvers, (b) horizontal rotary dissolvers, (c) pulsed dissolvers, (d) external loop air-lift reactor, (e) tumbling inclined dissolvers, etc. The continuous category includes (a) moving bed dissolvers, (b) rotary screw dissolvers, (c) pulsed dissolvers, (d) rotary bucket dissolvers, etc. A critical analysis of all these types is needed to bring out the suitability of a particular design for a given dissolution operation. One such methodology has been suggested in 7(c) and 7(d) below.
 - (b) The design parameters include (a) solid hold-up, (b) critical energy requirement for solid suspension/active-movement, (c) mass transfer coefficient, and (d) the residence time distribution of solid phase. Although this information is available for stirred reactors (Mahajani and Joshi 1988, Rewatkar et al. 1991a, Rance et al. 2000, Pangarkar et al. 2002, Kumaresan and Joshi 2006), scant information is available for other reactors. Future research work is needed to include these aspects of reactor design.
 - (c) The present review focuses on the determination of rate-controlling step and the estimation of overall rate of reaction. For this purpose, a detailed procedure has been discussed for establishing intrinsic kinetics and the rates of mass transfer. From this knowledge of individual rates, the procedure for the estimation of overall rate of reaction has been given by Doraiswamy and Sharma (1984), Joshi et al. (1985), and Albright (2008).

These publications also describe a method for the optimum design. In brief, the following steps are used: (i) One begins with a certain set of parameters (temperature, pressure, inlet HNO_3 concentration and its percentage excess with respect to solids to be dissolved, particle size, surface area, etc.). One also begins with one of the reactor choices (say, three phase sparged reactor (Joshi et al. 1985)) and its diameter. (ii) The overall rates are estimated at practically all points in the reactor, and total performance is estimated with respect to height. Thus, we get reactor height with respect to extent of solid phase conversion. (iii) After getting the reactor dimensions, the capital cost and operating costs are estimated, from which the total annualized cost is calculated. This procedure is repeated to understand the sensitivity of all the abovementioned parameters on the total cost and gives sufficient data set for the optimum design.

- (d) In the execution of step (c), one needs the knowledge of (i) solid-liquid mass transfer coefficient at every location; (ii) profiles of solid phase, HNO_3 concentration, and temperature; (iii) axial dispersion coefficient; (iv) critical power consumption for the onset of solid suspension; etc. For the estimation of these design parameters, a large number of correlations are available in the published literature (Joshi and Sharma 1978, Joshi et al. 1980, Pandit and Joshi 1984, 1986, Raghav Rao and Joshi 1988, Raghava Rao et al. 1988, Joshi et al. 1990, Rewatkar et al. 1991b, Abraham et al. 1992, Nigam and Schumpe 1996, Patwardhan and Joshi 1998, Thompson and Doraiswamy 1999, Murli et al. 2007, Murthy et al. 2007, Kalaga et al. 2012). The handbooks in chemical engineering (Green and Perry 1999, Albright 2008) have given many more correlations. The limitation of empirical correlations is known now, and, therefore, in the recent past, correlations have been developed using artificial intelligence (Gandhi et al. 2008, 2007, Gupta et al. 2009, Gandhi and Joshi 2010a,b). The important difficulty in accurate estimate of design parameters is the complexity of three-dimensional turbulent multiphase flow. Although some efforts are available in the published literature, for instance (Bale et al. 2017), substantial additional work is needed to understand the transport phenomena in the vicinity of solid-fluid interface and in the bulk of carrier phase.

6.1 List of experiments to be performed

The following are the conditions under which more experiments should be conducted:

1. Nitric acid concentration: High acid region is typically in the range of 6–12 M nitric acid, which is what we encounter during reprocessing.
2. Effect of mass transfer: The experiments at 0–100 rpm are important for UO_2 and MOX with high U content.
3. Pellet: Pellets of different particle sizes have to be fabricated to simulate the actual conditions of spent fuel dissolution wherein the fuel is bound to be more porous due to the formation of gaseous FPs formed within the fuel matrix.
4. MOX fuel Pellets: Similarly, dissolution experiments should be conducted with MOX fuel pellets of varied composition similar to those expected in the spent fuel to understand the effect of chemical composition of the fuel on their dissolution rate.
5. Role of NO_x : It has been observed that stirring the reaction mixture reduces the dissolution rate as it drives the NO_x gas required for the dissolution away from the interface. But to increase the pellet surface area, it is required to tumble the fuel materials to break them down. Hence, to compensate for this, we can supply NO_x gas externally by sparging NO_2 into the reaction mixture. So some experiments with NO_2 sparging with and without mixing needs to be carried out to understand the overall dynamics of this.
6. Pellets with FPs: Some pellets with certain major fission product elements incorporated in them in appropriate concentrations have to be fabricated and subjected to dissolution to understand the effect of these metal atoms on the dissolution kinetics.
7. Role of additive: The experiments to investigate dissolution rates of PuO_2 , ThO_2 , and MOX need to be designed with the following additives in concentrated nitric acid: 0.001–0.05 M HF, 0.01–0.05 M Ag(II), 0.01–0.05 M Ce (IV), and 0.01–0.05 M Co(II).
8. Temperature: The experiments at boiling point of HNO_3 or near boiling point of HNO_3 should be performed for PuO_2 , ThO_2 , and MOX.

7 Conclusion

In this work, we have reviewed and analyzed existing literature on the dissolution of three oxides. The roles of additives, surface area, and temperature have been reviewed. Although there are several studies in the existing literature, the available information on the dissolution

of three important oxides is far from complete for the process development and design. Particularly, it has been observed that information on mass-transfer and overall rate model is not available in the existing literature. This information plays an important role in process development and design. Furthermore, the analysis of kinetics data suggests that the role of particle size, effective surface, and porosity should be included in quantitative models, in addition to intrinsic kinetics and mass-transfer models for better understanding of dissolution process.

For future works, suggestions have been made so that the gaps in the literature can be filled to develop a reliable process model for designing industrial dissolvers. The suggestions have been made in two directions: (i) model-based analysis of experimental data obtained from optimal design of experiments and (ii) the design of industrial dissolvers. Although the recommendations in this work are based on the analysis of the published data related to dissolution of nuclear materials, some of the recommendations may be useful for dissolution of non-nuclear materials in the acid.

Acknowledgments: Desigan acknowledges the support provided by the reprocessing group staff members of IGCAR and that of HBNI for providing a platform to perform his research on dissolution. Nirav Bhatt acknowledges the financial support from Department of Science and Technology, India, through INSPIRE Faculty scheme.

References

- Abraham M, Khare AS, Sawant SB, Joshi JB. Critical gas velocity for suspension of solid particles in three-phase bubble columns. *Ind Eng Chem Res* 1992; 31: 1136–1147.
- Ackerman JP. Chemical basis for pyrochemical reprocessing of nuclear fuel. *Ind Eng Chem Res* 1991; 30: 141–145.
- Albright L. *Albright's chemical engineering handbook*, Boca Raton, USA: CRC Press, 2008.
- Aneheim E. Development of a solvent extraction process for group actinide recovery from used nuclear fuel, Chalmers University of Technology, 2012.
- Baena A, Cardinaels T, Vos B, Binnemans K, Verwerf M. Synthesis of UO_2 and ThO_2 doped with Gd_2O_3 . *J Nucl Mater* 2015; 461(Supplement C): 271–281.
- Bale S, Sathe M, Ayeni O, Berrouk AS, Joshi JB, Nandakumar K. Spatially resolved mass transfer coefficient for moderate Reynolds number flows in packed beds: wall effects. *Int J Heat Mass Transfer* 2017; 110: 406–415.
- Barney GS. The kinetics of plutonium oxide dissolution in nitric/hydrofluoric acid mixtures. *J Radioanal Nucl Chem* 1977; 39: 1665–1669.
- Beaudoux X, Virot M, Chave T, Leturcq G, Clavier N, Dacheux N, Nikitenko SI. Catalytic dissolution of ceria–lanthanide mixed oxides provides environmentally friendly partitioning of lanthanides and platinum. *Hydrometallurgy* 2015; 151: 107–115.
- Benedict M, Pigford TH, Levi HW. *Nuclear Chemical Engineering*, Second Edition, McGraw-Hill Education, New York, 1981.
- Berger PA. Study of the dissolution mechanism by chemical and electrochemical oxidation-reduction of actinide oxides (UO_2 , NpO_2 , PuO_2 , and AmO_2) in an acid aqueous medium, 1990.
- Bjorklund CW, Staritzky E. Some observations on the reactivity of plutonium dioxide, USA, 1954.
- Bodansky D. Reprocessing spent nuclear fuel. *Phys Today* 2006; 80–81.
- Bourges J, Madic C, Koehly M, Lecomte M. Removal of alpha emitters from solid radioactive waste. *J Less-Common Met* 1986; 122: 303–308.
- Bray LA, Ryan JL, Wheelwright EJ. Dissolution of plutonium dioxide using HCl-HF, Report, Pacific Northwest Laboratory, USA, 1986.
- Carnal C, Hardy J, Lewis B. Simulation of a continuous rotary dissolver, USA: Office of Scientific and Technical Information, 1989.
- Casella A, Hanson B, Miller W. The effect of fuel chemistry on UO_2 dissolution. *J Nucl Mater* 2016; 476: 45–55.
- Chatterjee I, Joshi JB. Modeling, simulation and optimization: mono pressure nitric acid process. *Chem Eng J* 2008; 138: 556–577.
- Claparede L, Clavier N, Dacheux N, Mesbah A, Martinez J, Szenknect S, Moisy P. Multiparametric dissolution of thorium–cerium dioxide solid solutions. *Inorg Chem* 2011a; 50: 11702–11714.
- Claparede L, Clavier N, Dacheux N, Moisy P, Podor R, Ravoux J. Influence of crystallization state and microstructure on the chemical durability of cerium–neodymium mixed oxides. *Inorg Chem* 2011b; 50: 9059–9072.
- Claparede L, Tocino F, Szenknect S, Mesbah A, Clavier N, Moisy P, Dacheux N. Dissolution of $\text{Th}_{1-x}\text{U}_x\text{O}_2$: effects of chemical composition and microstructure. *J Nucl Mater* 2015; 457: 304–316.
- Cleveland JM. Chemistry of plutonium, Technical Report, 1970.
- COE, Processing of used nuclear fuel. <http://www.world-nuclear.org/information-library/nuclear-fuel-cycle/fuel-recycling/processing-of-used-nuclear-fuel.aspx>; 2017.
- Cooley CR. Status of electrolytic dissolution for LMFBR fuels, 1971.
- Cordara T, Szenknect S, Claparede L, Podor R, Mesbah A, Lavalette C, Dacheux N. Kinetics of dissolution of UO_2 in nitric acid solutions: a multiparametric study of the non-catalysed reaction. *J Nucl Mater* 2017; 496: 251–264.
- Corkhill CL, Myllykyla E, Bailey DJ, Thornber SM, Qi J, Maldonado P, Stennett MC, Hamilton A, Hyatt NC. Contribution of energetically reactive surface features to the dissolution of CeO_2 and ThO_2 analogues for spent nuclear fuel microstructures. *ACS Appl Mater Interfaces* 2014; 6: 12279–12289.
- Corkhill CL, Bailey DJ, Tocino FY, Stennett MC, Miller JA, Provis JL, Travis KP, Hyatt NC. Role of microstructure and surface defects on the dissolution kinetics of CeO_2 , a UO_2 fuel analogue. *ACS Appl Mater Interfaces* 2016; 8: 10562–10571.
- De Regge P, Huys D, Ketels J, Vandeveld L, Baetsle LH. Dissolution of mechanically mixed UO_2 – PuO_2 and insoluble residue characteristics, UK: Society of Chemical Industry, 1980.
- Demuth SF. Conceptual design for separation of plutonium and gallium by solvent extraction, USA: Los Alamos National Laboratory, 1997.
- Desigan N, Augustine E, Murali R, Pandey N, Mudali UK, Natarajan R, Joshi JB. Dissolution kinetics of Indian PHWR natural UO_2 fuel pellets in nitric acid – effect of initial acidity and temperature. *Prog Nucl Energy* 2015a; 83: 52–58.

- Desigan N, Panday NK, Mudali UK. Effect of nitrous acid on the dissolution kinetics of UO_2 pellets in nitric acid, CHEMNUT 2015, IGCAR, India, 2015b.
- Desigan N, Bhatt N, Pandey N, Mudali UK, Natarajan R, Joshi JB. Mechanism of dissolution of nuclear fuel in nitric acid relevant to nuclear fuel reprocessing. *J Radioanal Nucl Chem* 2017; 312: 141–149.
- Dickinson C, Heal G. Solid–liquid diffusion controlled rate equations. *Thermoch Acta* 1999; 340–341: 89–103.
- Doraiswamy L, Sharma M. Heterogeneous reactions: analysis examples and reactor design. Vol. 1: gas solid and solid-solid reactions, New York, NY: John Wiley and Sons, 1984.
- Etter DE, Herald WR. Plutonium-238 dioxide dissolution study, USA: Department of Energy, 1974.
- Eung-Ho K, Doo-Sung H, Jae-Hyung Y. Dissolution mechanism of UO_2 in nitric acid solution by photochemical reaction. *J Radioanal Nucl Chem* 2000; 245: 567–570.
- Fallet A, Larabi-Gruet N, Jakab-Costenoble S, Moisy P. Electrochemical behavior of plutonium in nitric acid media. *J Radioanal Nucl Chem* 2016; 308: 587–598.
- Fife KW. A kinetic study of plutonium dioxide dissolution in hydrochloric acid using Iron(II) as an electron transfer catalyst. PhD. Thesis, USA, 1996.
- Fisher FD. The SULFEX process terminal development report. General Electric Co., Hanford Atomic Products Operation, Richland, Washington. AEC Research and Development Report HW-66439, 1960.
- Forsyth R, Werme L. Spent fuel corrosion and dissolution. *J Nucl Mater* 1992; 190: 3–19.
- Fukasawa T, Ozawa Y. Relationship between dissolution rate of uranium dioxide pellets in nitric acid solutions and their porosity. *J Radioanal Nucl Chem* 1986; 106: 345–356.
- Gandhi AB, Joshi JB. Estimation of heat transfer coefficient in bubble column reactors using support vector regression. *Chem Eng J* 2010a; 160: 302–310.
- Gandhi AB, Joshi JB. Unified correlation for overall gas hold-up in bubble column reactors for various gas–liquid systems using hybrid genetic algorithm-support vector regression technique. *Can J Chem Eng* 2010b; 88: 758–776.
- Gandhi AB, Joshi JB, Jayaraman VK, Kulkarni BD. Data-driven dynamic modeling and control of a surface aeration system. *Ind Eng Chem Res* 2007; 46: 8607–8613.
- Gandhi A, Joshi JB, Kulkarni A, Jayaraman V, Kulkarni B. SVR-based prediction of point gas hold-up for bubble column reactor through recurrence quantification analysis of LDA time-series. *Int J Multiphase Flow* 2008; 34: 1099–1107.
- Gelis VM, Shumilova YB, Ershov BG, Maslennikov AG, Milyutin VV, Kharitonov OV, Logunov MV, Voroshilov YA, Bobritskii AV. Use of ozone for dissolving high-level plutonium dioxide in nitric acid in the presence of Am(V,VI) ions. *Radiochemistry* 2011; 53: 612–618.
- Goode J. Hot cell dissolution of highly irradiated 20% PuO_2 –80% UO_2 fast reactor fuel specimens, 1965.
- Green DW, Perry RH. Perry's chemical engineers' handbook, New York, USA: McGraw-Hill Professional, 1999.
- Grénman H, Ingves M, Wärna J, Corander J, Yu Murzin D, Salmi T. Common potholes in modeling solid–liquid reactions—methods for avoiding them. *Chem Eng Sci* 2011a; 66: 4459–4467.
- Grénman H, Salmi T, Murzin DY. Solid–liquid reaction kinetics – experimental aspects and model development. *Rev Chem Eng* 2011b; 27: 53–77.
- Gupta PP, Merchant SS, Bhat AU, Gandhi AB, Bhagwat SS, Joshi JB, Jayaraman VK, Kulkarni BD. Development of correlations for overall gas hold-up, volumetric mass transfer coefficient, and effective interfacial area in bubble column reactors using hybrid genetic algorithm support vector regression technique: viscous Newtonian and non-Newtonian liquids. *Ind Eng Chem Res* 2009; 48: 9631–9654.
- Hanson BD. The burnup dependence of light water reactor spent fuel oxidation, Technical Report; Richland, WA, USA: Pacific Northwest National Lab., 1998.
- Harmon HD. Dissolution of PuO_2 with cerium (IV) and fluoride promoters, USA, 1975a.
- Harmon HD. Evaluation of fluoride, cerium (IV), and cerium(IV)-fluoride mixtures as dissolution promoters for PuO_2 scarp recovery processes, 1975b.
- Heisbourg G, Hubert S, Dacheux N, Ritt J. The kinetics of dissolution of $\text{Th}_{1-x}\text{U}_x\text{O}_2$ solid solutions in nitric media. *J Nucl Mater* 2003; 321: 141–151.
- Heisbourg G, Hubert S, Dacheux N, Purans J. Kinetic and thermodynamic studies of the dissolution of thoria-uranium solid solutions. *J Nucl Mater* 2004; 335: 5–13.
- Hill C, Berthon L, Bros P, Dancausse J, Guillaneux D. SANEX-BTP process development studies. *J Nucl Sci Technol* 2002; 39(sup 3): 309–312.
- Horlait D, Claparede L, Clavier N, Szenknect S, Dacheux N, Ravaut J, Podor R. Stability and structural evolution of $\text{Ce(IV)}_{1-x}\text{Ln(III)}_x\text{O}_{2-x/2}$ solid solutions: a coupled m-Raman/XRD approach. *Inorg Chem* 2011; 50: 7150–7161.
- Horlait D, Tocino F, Clavier N, Dacheux N, Szenknect S. Multiparametric study of $\text{Th}_{1-x}\text{Ln}_x\text{O}_{2-x/2}$ mixed oxides dissolution in nitric acid media. *J Nucl Mater* 2012; 429: 237–244.
- Horlait D, Claparede L, Tocino F, Clavier N, Ravaut J, Szenknect S, Podor R, Dacheux N. Environmental SEM monitoring of $\text{Ce}_{1-x}\text{Ln}_x\text{O}_{2-x/2}$ mixed-oxide microstructural evolution during dissolution. *J Mater Chem A* 2014; 2: 5193–5203.
- Horner D, Crouse D, Mailen J. Cerium-promoted dissolution of PuO_2 and PuO_2 – UO_2 in nitric acid, 1977.
- Hubert S, Barthelet K, Fourest B, Lagarde G, Dacheux N, Baglan N. Influence of the precursor and the calcination temperature on the dissolution of thorium dioxide. *J Nucl Mater* 2001; 297: 206–213.
- Hubert S, Heisbourg G, Dacheux N, Moisy P. Effect of inorganic ligands and hydrogen peroxide on ThO_2 dissolution. Behaviour of $\text{Th}_{0.87}\text{Pu}_{0.13}\text{O}_2$ during leaching test. *Inorg Chem* 2008; 47: 2064–2073.
- Hyder ML, Prout W. Dissolution of thorium oxide. Savannah River Lab, USA, 1966.
- Ikeda Y, Yasuike Y, Nishimura K, Hasegawa S, Takashima Y. Kinetic study on dissolution of UO_2 powders in nitric acid. *J Nucl Mater* 1995; 224: 266–272.
- Inoue A, Tsujino T. Dissolution rates of uranium oxide (U_3O_8) powders in nitric acid. *Ind Eng Chem Process Des Dev* 1984; 23: 122–125.
- Jégou C, Caraballo R, De Bonfils J, Broudic V, Peugot S, Vercoeur T, Roudil D. Oxidizing dissolution of spent MOX47 fuel subjected to water radiolysis: solution chemistry and surface characterization by Raman spectroscopy. *J Nucl Mater* 2010; 399: 68–80.
- Joshi JB, Sharma M. Liquid phase back mixing in sparged contactors. *Can J Chem Eng* 1978; 56: 116–119.

- Joshi JB, Sharma M, Shah Y, Singh C, Ally M, Klinzing G. Heat transfer in multiphase contactors. *Chem Eng Commun* 1980; 6: 257–271.
- Joshi JB, Mahajani VV, Juvekar VA. Invited review absorption of NO_x gases. *Chem Eng Commun* 1985; 33: 1–92.
- Joshi JB, Patil T, Ranade V, Shah Y. Measurement of hydrodynamic parameters in multiphase sparged reactors. *Rev Chem Eng* 1990; 6: 73–227.
- Juillet F, Adnet J, Gasgnier M. Ultrasound effects on the dissolution of refractory oxides (CeO_2 and PuO_2) in nitric acid. *J Radioanal Nucl Chem* 1997a; 224: 137–143.
- Juillet F, Adnet JM, Gasgnier M. Ultrasound effects on the dissolution of refractory oxides (CeO_2 and PuO_2) in nitric acid. *J Radioanal Nucl Chem* 1997b; 224: 137–143.
- Kalaga DV, Reddy RK, Joshi JB, Dalvi SV, Nandkumar K. Liquid phase axial mixing in solid–liquid circulating multistage fluidized bed: CFD modeling and RTD measurements. *Chem Eng J* 2012; 191: 475–490.
- Kazanjan AR, Stevens JR. Dissolution of plutonium oxide in nitric acid at high hydrofluoric acid concentrations, Oak Ridge Tennessee, USA: Department of Energy, 1984.
- Keshtkar AR, Abbasizadeh S. Activation energy determination and kinetic modeling of thorium oxide dissolution in nitric acid/hydrofluoric acid system: influence of fluoride ion on ThO_2 dissolution. *Prog Nucl Eng* 2016; 93: 362–370.
- Kim HS, Joung CY, Lee BH, Oh JY, Koo YH, Heimgartner P. Applicability of CeO_2 as a surrogate for PuO_2 in a MOX fuel development. *J Nucl Mater* 2008; 378: 98–104.
- Kumaresan T, Joshi JB. Effect of impeller design on the flow pattern and mixing in stirred tanks. *Chem Eng J* 2006; 115: 173–193.
- Laidler J, Battles J, Miller W, Ackerman J, Carls E. The technology of the integral fast reactor and its associated fuel cycle development of pyroprocessing technology. *Prog Nucl Eng* 1997; 31: 131–140.
- Levenspiel O. Chemical reaction engineering, 3rd ed., USA: John Wiley & Sons, 1999.
- Machuron-Mandard X, Madic C. Basic studies on the kinetics and mechanism of the rapid dissolution reaction of plutonium dioxide under reducing conditions in acidic media. *J Alloys Compd* 1994; 213: 100–105.
- Madic C, Berger P, Machuron-Mandard X. Mechanisms of the rapid dissolution of plutonium dioxide in acidic media under oxidizing and reducing conditions. *Transuranium elements – a half century*, American Chemical Soc., 1992.
- Mahajani VV, Joshi JB. Kinetics of reactions between carbon dioxide and alkanolamines. *Gas Sep Purif* 1988; 2: 50–64.
- Marchenko VI, Dvoeglazov KN, Volk VI. Use of redox reagents for stabilization of Pu and Np valence forms in aqueous reprocessing of spent nuclear fuel: chemical and technological aspects. *Radiochemistry* 2009; 51: 329–344.
- Marquardt W. Model-based experimental analysis of kinetic phenomena in multi–phase reactive systems. *Chem Eng Res Des* 2005; 83: 561–573.
- Marra JC. Cerium as a surrogate in the plutonium immobilized form, Technical Report; Savannah River Site (US), 2001.
- Mason T, Paniwnyk L, Lorimer J. The uses of ultrasound in food technology. *Ultrason Sonochem* 1996; 3: S253–S260.
- Mineo H, Isogai H, Morita Y, Uchiyama G. An investigation into dissolution rate of spent nuclear fuel in aqueous reprocessing. *J Nucl Sci Tech* 2004; 41: 126–134.
- Miner FJ, Nairn JH, Berry JW. Dissolution of plutonium in dilute nitric acid. *Ind Eng Chem Product Res Dev* 1969; 8: 402–405.
- Moisy P, Nikitenko S, Venault L, Madie C. Sonochemical dissolution of metallic plutonium in a mixture of nitric and formic acid. *Radiochimica Acta* 1996; 75: 219–226.
- Moore RL, Goodall CA, Hepworth JL, Watts RA. Nitric acid dissolution of thorium. Kinetics of fluoride-catalyzed reaction. *Ind Eng Chem* 1957; 49: 885–887.
- Murli SV, Chavan PV, Joshi JB. Solid dispersion studies in expanded beds. *Ind Eng Chem Res* 2007; 46: 1836–1842.
- Murthy B, Ghadge R, Joshi JB. CFD simulations of gas–liquid–solid stirred reactor: prediction of critical impeller speed for solid suspension. *Chem Eng Sci* 2007; 62: 7184–7195.
- Myllykylä E, Lavonen T, Stennett M, Corkhill C, Ollila K, Hyatt N. Solution composition and particle size effects on the dissolution and solubility of a ThO_2 microstructural analogue for UO_2 matrix of nuclear fuel. *Radiochimica Acta* 2015; 103: 565–576.
- Natarajan R, Vijayakumar V, Subba Rao RV, Pandey NK. Experiences of reprocessing of plutonium-rich mixed carbide fuels. *J Radioanal Nucl Chem* 2015; 304: 401–407.
- Nigam K, Schumpe A. Three-phase sparged reactors, Amsterdam, Netherlands: Gordon & Breach, 1996.
- Nikitenko S, Venault L, Pflieger R, Chave T, Bisel I, Moisy P. Potential applications of sonochemistry in spent nuclear fuel reprocessing: a short review. *Ultrason Sonochem* 2010; 17: 1033–1040.
- Odom CH. Continuous or semi-continuous leacher for leaching soluble core material from sheared spent nuclear fuel tubes, USA: Office of Scientific and Technical Information, 1972.
- OECD, NEA/Organization for Economic Co-operation and Development Pyrochemical separations in nuclear applications: a status report, Paris, France, 2004.
- Olander D. Nuclear fuels – present and future. *J Nucl Mater* 2009; 389: 1–22.
- Órfão JM, Martins FG. Kinetic analysis of thermogravimetric data obtained under linear temperature programming—a method based on calculations of the temperature integral by interpolation. *Thermoch Acta* 2002; 390: 195–211.
- Pandit A, Joshi JB. Three phase sparged reactors-some design aspects. *Rev Chem Eng* 1984; 2: 1–84.
- Pandit A, Joshi JB. Mass and heat transfer characteristics of three phase sparged reactors. *Trans Instn Chem Engrs A: Chem Eng Res Des* 1986; 64: 125–157.
- Pangarkar VG, Yawalkar AA, Sharma MM, Beenackers AACM. Particle–liquid mass transfer coefficient in two-/three-phase stirred tank reactors. *Ind Eng Chem Res* 2002; 41: 4141–4167.
- Patwardhan AW, Joshi JB. Design of stirred vessels with gas entrained from free liquid surface. *Can J Chem Eng* 1998; 76: 339–364.
- Pierce R. Uranium metal dissolution in the presence of fluoride and boron, USA: Office of Scientific and Technical Information, 2004.
- Poinssot C, Ikeuchi H, Shibata A, Sano Y, Koizumi T. Dissolution behavior of irradiated mixed-oxide fuels with different plutonium contents. *Procedia Chem* 2012a; 7: 77–83.
- Poinssot C, Koyama T, Sakamura Y, Iizuka M, Kato T, Murakami T, Glatz JP. Development of pyro-processing fuel cycle technology for closing actinide cycle. *Procedia Chem* 2012b; 7: 772–778.
- Polley GM. Downblend and disposition remote handled U–233 material at the WIPP facility – 9374, 2009.

- Polyakov A, Zakharkin B, Rorisov L, Kucherenko V, Revjakin V, Bourges J, Boesch A, Capelle P, Bercegol H, Brossard P, Bros P, Sicard B, Bernard H. A/MOX: progress report on the research concerning the aqueous processes for allied plutonium conversion to PuO_2 or $(\text{U}, \text{Pu})\text{O}_2$, Global 1995.
- Popel A, Le Sollicet S, Lampronti G, Day J, Petrov P, Farnan I. The effect of fission-energy Xe ion irradiation on the structural integrity and dissolution of the CeO_2 matrix. *J Nucl Mater* 2017; 484: 332–338.
- Popel AJ, Wietsma TW, Engelhard MH, Lea AS, Qafoku O, Grygiel C, Monnet I, Ilton ES, Bowden ME, Farnan I. The effect of ion irradiation on the dissolution of UO_2 and UO_2 -based simulant fuel. *J Alloys Compd* 2018; 735: 1350–1356.
- Raghav Rao K, Joshi JB. Liquid phase mixing in mechanically agitated vessels. *Chem Eng Commun* 1988; 74: 1–25.
- Raghava Rao K, Rewatkar V, Joshi JB. Critical impeller speed for solid suspension in mechanically agitated contactors. *AIChE J* 1988; 34: 1332–1340.
- Rance P, Tinsley T, Raginsky L, Morkovnikov V. Pneumatically pulsed continuous dissolver for nuclear fuel reprocessing; Atalante 2000 – International Conference on Scientific Research on the Back-End of the Fuel Cycle for the 21st Century, Avignon, France, 2000.
- Rat B, Heres X. Modelling and achievement of a SANEX process flowsheet for trivalent actinides/lanthanides separation using BTP Extractant (bis-1,2,4-triazinyl-pyridine), 2004.
- Rewatkar VB, Raghava Rao KSMS, Joshi JB. Critical impeller speed for solid suspension in mechanically agitated three-phase reactors. 1. experimental part. *Ind Eng Chem Res* 1991a; 30: 1770–1784.
- Rewatkar VB, Rao KR, Joshi JB. Critical impeller speed for solid suspension in mechanically agitated three-phase reactors. 1. Experimental part. *Ind Eng Chem Res* 1991b; 30: 1770–1784.
- Romanovskiy VN, Smirnov IV, Babain VA, Todd TA, Herbst RS, Law JD, Brewer KN. The universal solvent extraction (UNEX) process. I. Development of the UNEX process solvent for the separation of cesium, strontium, and the actinides from acidic radioactive waste. *Solvent Extr Ion Exc* 2001; 19: 1–21.
- Ryan JL, Bray LA. Dissolution of plutonium dioxide—a critical review. *Am Chem Soc USA* 1980; 499–514.
- Ryan JL, Bray LA, Wheelwright EJ, Bryan GH. Catalyzed electrolytic plutonium oxide dissolution (CEPOD) the past seventeen years and future potential, 1990.
- Sakurai T, Takahashi A, Ishikawa N, Komaki Y. The composition of NO_x generated in the dissolution of uranium dioxide. *Nuclear Technology* 1988; 83: 24–30.
- Salmi T, Grénman H, Wärnå J, Murzin DY. Revisiting shrinking particle and product layer models for fluid–solid reactions – from ideal surfaces to real surfaces. *Chem Eng Process Process Intensification* 2011; 50: 1076–1084.
- Sano Y, Katsurai K, Washiya T, Koizumi T, Matsumoto S. Development of simulation code for FBR spent fuel dissolution with rotary drum type continuous dissolver; Proceedings of the ICONE-19 The 19th International Conference on Nuclear Engineering, Japan, 2011.
- Sasaki S, Wada Y, Tomiyasu H. Global environmental and nuclear energy systems–2 basic study of photochemistry for application to advanced nuclear fuel cycle technology. *Prog Nucl Eng* 1998; 32: 403–410.
- Schiefelbein GF, Lerch RE. Dissolution properties of UO_2 - PuO_2 thermal reactor fuels, 1971.
- Schulz W. Aqueous decladding and dissolution of plutonium recycle test reactor fuels. Part 2. PuO_2 - UO_2 fuels, USA: Office of Scientific and Technical Information, 1966.
- Serrano J, Glatz J, Toscano E, Papaioannou D, Barrero J, Coquerelle M. Influence of low temperature air oxidation on the dissolution behavior of UO_2 and MOX spent fuel. *J Alloys Comp* 1998; 271–273: 573–576.
- Shabbir M, Robins RG. Kinetics of the dissolution of uranium dioxide in nitric acid. I. *J Appl Chem* 1968; 18: 129–134.
- Shabbir M, Robins RG. Kinetics of the dissolution of uranium dioxide in nitric acid. II. *J Appl Chem* 1969; 19: 52–56.
- Shakila AM, Srinivasan TG, Sabharwal KN, Rao PRV. Dissolution of PuO_2 in HNO_3 - HF - N_2H_4 medium. *Nucl Technol* 1987; 79: 116.
- Shakila AM, Srinivasan TG, Sabharwal KN. Dissolution of PuO_2 in hydrochloric acid– effect of reducing agents. *Nucl Technol* 1989; 88: 290.
- Shirsat A, Ali M, Kolay S, Datta A, Das D. Transport properties of I, Te and Xe in Thoria–Urania sim fuel. *J Nucl Mater* 2009; 392: 16–21.
- Shying M, Florence T, Carswell D. Oxide dissolution mechanisms–I. *J Inorg Nucl Chem* 1970; 32: 3493–3508.
- Shying M, Florence T, Carswell D. Oxide dissolution mechanisms – II a mechanism for the thoria/nitric/hydrofluoric acid system. *J Inorg Nucl Chem* 1972; 34: 213–220.
- Sinkov SI, Lumetta GJ. Sonochemical digestion of high-fired plutonium dioxide samples, USA: PNNL-16035, 2006a.
- Sinkov SI, Lumetta GJ. Sonochemical digestion of high-fired plutonium dioxide samples. Technical Report; Richland, WA, USA: Pacific Northwest National Laboratory (PNNL), 2006b.
- Smith PW. The zirflex process terminal development report, Richland, Washington: General Electric Co., Hanford Atomic Products Operation, 1960.
- Sood DD, Patil SK. Chemistry of nuclear fuel reprocessing: current status. *J Radioanal Nucl Chem* 1996; 203: 547–573.
- Szenknect S, Mesbah A, Horlait D, Clavier N, Dourdain S, Ravaux J, Dacheux N. Kinetics of structural and microstructural changes at the solid/solution interface during dissolution of cerium (iv)–neodymium (iii) oxides. *J Phys Chem C* 2012; 116: 12027–12037.
- Tahara Y, Zhu B, Kosugi S, Ishikawa N, Okamoto Y, Hori F, Matsui T, Iwase A. Study on effects of swift heavy ion irradiation on the crystal structure in CeO_2 doped with Gd_2O_3 . *Nucl Instrum Methods Phys Res, Sect B* 2011; 269: 886–889.
- Takeuchi T, Kawamura K. The kinetic study of the reaction of thorium oxide with hydrofluoric acid. *J Inorg Nucl Chem* 1972; 34: 2497–2503.
- Takeuchi T, Hanson C, Wadsworth ME. Kinetics and mechanism of the dissolution of thorium oxide in hydrofluoric acid and nitric acid mixtures. *J Inorg Nucl Chem* 1971; 33: 1089–1098.
- Taylor RF, Sharratt EW, De Chazal LEM, Logsdail DH. Dissolution rates of uranium dioxide sintered pellets in nitric acid systems. *J Appl Chem* 1963; 13: 32–40.
- Thompson L, Doraiswamy L. Sonochemistry: science and engineering. *Ind Eng Chem Res* 1999; 38: 1215–1249.
- Thompson MC, Norato MA, Kessinger GF, Pierce RA, Rudisill TS, Johnson JD. Demonstration of the UREX solvent extraction process with Dresden reactor fuel solution; WSRC-TR-2002-00444 Revision 0, September 30, 2002.

- Tocino F, Szenknect S, Mesbah A, Clavier N, Dacheux N. Dissolution of uranium mixed oxides: the role of oxygen vacancies vs. the redox reactions. *Prog Nucl Energ* 2014; 72: 101–106.
- Uriate AL, Rainey RH. Dissolution of high-density UO_2 , PuO_2 , and UO_2 - PuO_2 pellets in inorganic acids, 1965.
- Virost M, Chave T, Horlait D, Clavier N, Dacheux N, Ravaux J, Nikitenko SI. Catalytic dissolution of ceria under mild conditions. *J Mater Chem* 2012; 22: 14734–14740.
- Virost M, Szenknect S, Chave T, Dacheux N, Moisy P, Nikitenko SI. Uranium carbide dissolution in nitric solution: sonication vs. silent conditions. *J Nucl Mater* 2013; 441: 421–430.
- Wada Y, Morimoto K, Tomiyasu H. Photochemical dissolution of UO_2 powder in nitric acid solution at room temperature. *Radiochim Acta* 1996; 72: 83–91.
- Wen CY. Noncatalytic heterogeneous solid-fluid reaction models. *Ind Eng Chem* 1968; 60: 34–54.
- Yu JF, Ji C. The kinetics of cobalt(II) extraction with EHEHPA in heptane mixed extraction systems. *Chem J Chin Univ* 1992; 13: 224–226.
- Zawodzinski C, Smith WH, Martinez KR. Kinetic studies of the electrochemical generation of Ag(II) ion and the catalytic oxidization of selected organics, USA: Los Alamos National Lab, 1993.